DEVELOPMENT OF CONTINUOUS-FLOW POLYMERASE CHAIN REACTION MICROCHIP WITH INTEGRATED ELECTROLYTIC PUMP

YIU CHUN YING

M.Phil.

THE HONG KONG POLYTECHNIC UNIVERSITY

2013

The Hong Kong Polytechnic University

Interdisciplinary Division of Biomedical Engineering

Development of Continuous-Flow Polymerase Chain Reaction Microchip with Integrated Electrolytic Pump

by

Yiu Chun Ying

A thesis submitted in partial fulfillment of

requirements for the degree of

Master of Philosophy

August 2012

Certificate of Originality

I hereby declare that this thesis is my own work and that, to the best of my knowledge and belief, it reproduces no material previously published or written, nor material that has been accepted for the award of any other degree or diploma, except where due acknowledgement has been made in the text.

_____ (Signed)

Mr. Yiu Chun Ying (Name of Student)

Abstract

There has been huge demand for point-of-care and on-site nucleic acid analysis. Microfluidic devices or microchips have received considerable attention thanks to their high portability, simple operation, short assay time, and low cost. One important module is deoxyribonucleic acid (DNA) amplification as the amount of nucleic acid sample is usually too little for direct detection. Particularly useful for this task is continuous-flow polymerase chain reaction (CFPCR), which enables high-speed PCR by passing an amplification reaction mixture through a microchannel to achieve the required repeated thermal cycling. Up until now, the fluidic flow had been controlled off-chip by bulky syringe pump, thereby seriously affecting the portability of the microchip device. To address this issue, herein, a CFPCR microchip with integrated on-chip electrolytic pump was developed.

The CFPCR microchip comprised an electrolytic pumping chamber, PCR reagent reservoir, oil reservoir, and microchannel for PCR thermal cycling. The chamber, reservoir, and microchannel were made from a polydimethylsiloxane substrate. Platinum electrodes for the electrolytic pump were patterned onto a glass substrate, which was then plasma-bonded to and thus sealed the polydimethylsiloxane substrate. A feedback control system was custom-built to achieve accurate PCR thermal cycling (±1 °C).

Gas bubbles generated from the on-chip electrolytic pump with constant voltage control successfully drove PCR reagent through the microchannel. CFPCR could be completed in ~20 min with the PCR product visible by gel electrophoresis. In addition, the effects of other key parameters, which included addition of silicone oil, concentration of Taq DNA polymerase, and dynamic/static passivation with bovine serum albumin on DNA amplification efficiency were studied. In fact, the on-chip electrolytic pump could also be driven by constant current and provide a more stable fluid flow than constant voltage control.

This work successfully demonstrated the use of on-chip electrolytic pump to achieve fluidic control for CFPCR. Other functional modules such as sample preparation and product detection can be readily integrated to realize a portable device for decentralized nucleic acid analysis.

Acknowledgements

I would like to express my great appreciation to my supervisor, Dr. Thomas Ming-Hung Lee, for his valuable and constructive suggestions throughout my study. His critical and novel thinking always trigger me to think and explore more. Without his patience, motivation, and guidance, I cannot come up with the present progress. In this study, I learned the skills and attitude to deal with problems which would be beneficial to my whole life. I really enjoy this study and thanks for giving me the chance!

I would also like to take this opportunity to express my sincere thanks to my co-supervisor, Prof. Kai-Leung Yung, and my friends/colleagues Jacky Wong, Cristina Leung, Derek Lee, Anthony Wong, Samy Leung, Baojian Xu, Brian Pow, and Zongbin Liu at The Hong Kong Polytechnic University for their support and help throughout my study. In addition, I would like to thank Xiaoteng Luo at The Hong Kong University of Science and Technology for his help in the sputtering of platinum electrodes.

Finally, I would like to express my special thanks to my father, mother, and brother for their endless loves.

Table of Contents

Title ii

Certificate of Originality iii

Supervisor/Co-Supervisor Signatures iv

Abstract v

Acknowledgements vii

Table of Contents viii

List of Figures xii

List of Tables xviii

List of Abbreviations xix

1. Introduction 1

1.1 Background 1

1.2 Literature Review 2

1.2.1 Polymerase Chain Reaction 3

1.2.2 Microchip-Based PCR 4

1.2.3 Surface Passivation 14

1.2.4 Microfluidic Control 17

1.3 Objectives 26

2. Methodology 27

2.1 CFPCR Microchip 27

2.1.1 Design of CFPCR Microchip 27

2.1.2 Fabrication of CFPCR Microchip 33
2.2 Electrolytic Pump 35
2.2.1 Design of Electrolytic Pump 35
2.2.2 Fabrication of Electrolytic Pump.....37
2.2.3 Control of the Electrolytic Pump……38
2.3 Bonding of CFPCR and Electrolytic Pump Microchip. 43
2.4 Temperature Control System.....44
2.4.1 Design of Temperature Control System 44
2.4.2 Fabrication of Temperature Control System 46
2.4.3 Calibration of Temperature Control System 49
2.5 PCR Experiment.....49
2.5.1 PCR Protocol 50
2.5.2 Experimental Setup 50
2.5.2.1 Effect of Silicone Oil.....52
2.5.2.2 Effect of Concentration of Taq DNA Polymerase 52
2.5.2.3 Effect of Surface Passivation.....52
2.5.2.4 Effect of CFPCR Duration 53
2.5.2.5 Performance of Electrolytic Pump 53
2.5.3 Agarose Gel Electrophoresis 54
3. Results 55
3.1 Fluidic Flow.....55
3.1.1 Gas Bubbles Generation 55
3.1.2 Control of the Electrolytic Pump using Voltage Source 56

3.1.3 Control of the Electrolytic Pump using Current Source.....59
3.1.4 Fluidic Flow in CFPCR.....60
3.2 Temperature Control.....62
3.3 PCR Experiment.....63
3.3.1 Effect of Silicone Oil.....63
3.3.2 Effect of Concentration of Taq DNA Polymerase.....64
3.3.3 Effect of Surface Passivation.....65
3.3.4 Effect of CFPCR Duration.....66
3.3.5 Performance of Electrolytic Pump.....67
4. Discussion.....69
4.1 Fluidic Flow.....69
4.1.1 Gas Bubbles Generation.....69
4.1.2 Control of the Electrolytic Pump using Voltage Source.....69
4.1.3 Control of the Electrolytic Pump using Current Source.....70
4.1.4 Fluidic Flow in CFPCR.....70
4.2 Temperature Control.....71
4.3 PCR Experiment.....72
4.3.1 Effect of Silicone Oil.....72
4.3.2 Effect of Concentration of Taq DNA Polymerase.....73
4.3.3 Effect of Surface Passivation.....73
4.3.4 Effect of CFPCR Duration.....74
4.3.5 Performance of Electrolytic Pump.....75
5. Conclusions and Recommendations.....76

5.1 Conclusions 76

5.2 Recommendations for Future Work 77

References 79

List of Figures

Figure 1.1 A schematic diagram of the PCR showing the three key temperature steps.. 3

Figure 1.2 A cross-sectional view of the stationary microchip-based PCR developed by Northrup *et al.* in 1993.. 4

Figure 1.3 A sketch of two-chamber PCR microchip developed by Poser *et al*. The microchip consisted of 3 layers: a) cover; b) topside; c) backside; and 7 components: 1) inlet; 2) cover; 3) adjustment; 4) reaction chamber; 5) air chamber; 6) thin-film heater; 7) temperature sensor..... 5

Figure 1.4 A schematic diagram for the plastic fluidic chip developed by Liu et al..6

Figure 1.5 A continuous-flow PCR in glass chip developed by Kopp *et al.* in 1998.9

Figure 1.6 (A) Gel electrophoresis results of the CFPCR by Kopp *et al.* Lane 1 is the control with conventional thermocycler; lanes 2 to 8 are the CFPCR with decreasing thermocycling duration from 18.8 to 1.5 min. (B) Fluorescence signals of the CFPCR products against thermocycling duration.. 10

Figure 1.7 Assembly of the closed-loop CFPCR. Block with control channels at the bottom surface (top layer), thin layer with fluid channel at the bottom surface and glass coverslip (middle layer), and heaters with leads on a glass substrate (bottom layer). Arrows indicate the air and fluid through-holes.. 11

Figure 1.8 A schematic structure of the oscillatory CFPCR by Wang *et al.*..... 12

Figure 1.9 Effect of linear velocity on the generation of a 500-bp PCR product. Lanes 1 and 5 are DNA size markers; lanes 2–4 are the CFPCR products at cycle rates of 7.8, 5.2, and 3.9 s/cycle, respectively 13

Figure 1.10 Photograph of the setup for a continuous-flow reverse transcription-PCR system with fluorescence detection 14

Figure 1.11 Gel electrophoresis image of PCR results from Wilding *et al.* Lanes 1 and lane are DNA size marker; lanes 2 is PCR performed by thermal cycler; lanes 3 and 4 are PCR performed by microchip. 14

Figure 1.12 Gel electrophoresis results showing the effects of material and surface area on PCR inhibition by Erill *et al*. 15

Figure 1.13 Micropumps with different actuation methods. 19

Figure 1.14 Schematic diagram showing the principle of electrokinetic synchronized cyclic continuous-flow PCR process. (a) Sample was filled into reservoir 5, and 800 V was applied to the electrodes in reservoirs 5 and 6. (b) One cycle included four steps. The DNA plug was driven when the 1.5 kV was applied to different pairs of electrodes…….....22

Figure 1.15 An electrolytically actuated drug delivery device by Li *et al*.. 24

Figure 1.16 Schematic illustration showing the flow (top) with PCR reagents and fluorinated oil and (bottom) with PCR reagents only. 25

Figure 1.17 (a–c) Bubble elimination with paraffin oil plugs at both the anterior and posterior ends of the ink plug. (d–e) Bubble was generated without the paraffin oil plugs. (f) PCR sample with the paraffin oil plugs 25

Figure 2.1 A CFPCR device consists of CFPCR microchip (top layer), electrolytic pump (middle layer), temperature control system (bottom)..... 28

Figure 2.2 A CFPCR microchip consisting of four main regions: pumping chamber, PCR reservoir, oil reservoir and PCR region. 28

Figure 2.3 Detailed dimensions (expressed in mm) of the CFPCR microchip. 29

Figure 2.4 PCR reaction region consists of four regions: initial denaturation, denaturation, annealing, and extension. There are 40 thermal cycles for the CFPCR. The ratio of the denaturation, extension, and annealing are about 1:2:1..... 31

Figure 2.5 Diagram showing the fluidic flow within the microchip. 32

Figure 2.6 Microchannel with curved turns..... 33

Figure 2.7 Schematic illustrating the CFPCR microchip fabrication procedures using soft lithographic technique..... 34

Figure 2.8 A photograph showing the PDMS CFPCR microchip..... 34

Figure 2.9 A pair of interdigitated Pt electrodes for the electrolysis of water. 36

Figure 2.10 Detailed dimensions (expressed in mm) of the electrolytic pump. 36

Figure 2.11 Schematic illustrating the electrolytic pump microchip fabrication procedures using lift-off process 37

Figure 2.12 A photograph showing the electrolytic pump microchip. 38

Figure 2.13 Circuit diagram for the constant current circuit……...……39

Figure 2.14 Front panel of the LabVIEW ……40

Figure 2.15 Calculation of the error in PID……..…40

Figure 2.16 Calculation of the proportional component in PID……..…41

Figure 2.17 Calculation of the derivative component in PID……..…41

Figure 2.18 Calculation of the integral component and the output value in PID….42

Figure 2.19 Block diagram of the whole PID control. Current Input measured the applied current to the electrolytic pump. PID calculated the output voltage to the LM334 base on the measured current. Output Voltage measured the applied voltage to the LM334. To Excel wrote data (Applied current to the electrolytic pump and applied voltage to the LM334) to the excel file……42

Figure 2.20 A photograph showing the bonded CFPCR and electrolytic pump microchips.. 44

Figure 2.21 Design of the temperature control system..... 45

Figure 2.22 A flow chart illustrating the temperature control system for the CFPCR device..... 45

Figure 2.23 Detailed dimensions (expressed in mm) of the heating elements. (top) Cross-sectional and (bottom) top views. 46

Figure 2.24 Circuit diagram for the temperature control system. 47

Figure 2.25 A photograph showing the heaters. 48

Figure 2.26 A photograph showing the circuit of the temperature control system. 48

Figure 2.27 A photograph showing the CFPCR microchip with syringe..... 51

Figure 2.28 A photograph showing the syringe pump 51

Figure 2.29 A photograph showing the setup of the CFPCR with electrolytic pump. 54

Figure 3.1 A photograph showing the gas bubbles generated by the electrolytic pump. 55

Figure 3.2 Plot of average duration of cycle against the speed of syring pump…...56

Figure 3.3 Plot of duration of CFPCR against voltage applied to the electrolytic pump …….57

Figure 3.4 Plot of duration in each cycle using electrolytic pump with constant voltage ……..58

Figure 3.5 Plot of current against time when a constant voltage (3 V) was applied to the electrolytic pump ……...…58

Figure 3.6 Plot of duration in each cycle using electrolytic pump with different currents……..59

Figure 3.7 Plot of average duration of each cycle against current applied to the electrolytic pump……...60

Figure 3.8 A photograph showing the leakage of PCR reagents during the CFPCR. The green PCR reagents leaked out through the space between the glass and PDMS. 60

Figure 3.9 A photograph of the air gaps formed in the CFPCR microchannel 61

Figure 3.10 A photograph showing air trapped within the reservoir after sealing the inlets with polyimide film tape **……..……...**61

Figure 3.11 Plots of temperature against square of voltage of the three heaters/metal blocks..... 62

Figure 3.12 Plots of temperature of the three metal blocks against time. The time required for the metal blocks to reach the denaturation, annealing, and extension temperatures were 20, 25, and 25 min, respectively. 63

Figure 3.13 Gel electrophoresis image of the amplification results of CFPCR with different concentrations of Taq DNA polymerase. Lane 1 is DNA size marker; lanes 2, 3, and 4 are CFPCR with 0.5, 1.5, and 2.5 units/20 μL Taq DNA polymerase.. . 64

Figure 3.14 Gel electrophoresis image of the amplification results of CFPCR with dynamic passivation using different concentrations of BSA. Lane 1 is DNA size marker; lanes 2, 3, and 4 are CFPCR with 2, 0.5, and 0 μg/μL BSA..... 65

Figure 3.15 Gel electrophoresis image of the amplification results of CFPCR with static passivation. Lane 1 is DNA size marker; lanes 2, 3, and 4 are CFPCR with 0, 2, and 5 μg/μL BSA, respectively 66

Figure 3.16 Gel electrophoresis image of the amplification results of CFPCR with different durations using syringe pump. Lane 1 is DNA size marker; lanes 2 and 3 are CFPCR of 32 and 20 min, respectively. 67

Figure 3.17 Gel electrophoresis image of the amplification results of CFPCR using electrolytic pump. Lane 1 is DNA size marker; lane 2 is CFPCR using electrolytic pump.…….68

List of Tables

Table 1.1 Comparisons of CFPCR microchip……7

Table 1.2 Taq DNA polymerase adsorption in various materials using contact angle measurement……..16

Table 1.3 Mechanical micropumps for PCR microchips…….....20

Table 1.4 Non-mechanical micropumps……..….21

List of Abbreviations

bp	base pair
CFPCR	continuous-flow polymerase chain reaction
DNA	deoxyribonucleic acid
MEMS	microelectromechanical systems
PCR	polymerase chain reaction
PDMS	polydimethylsiloxane
PEG	polyethylene glycol
Pt	platinum
PVP	polyvinylpyrrolidone
RT-PCR	reverse transcription polymerase chain reaction
TBE	tris-borate-EDTA
Teflon	polytetrafluoroethylene
Ti	titanium

CHAPTER 1

INTRODUCTION

The demands for point-of-care and on-site nucleic acid analysis have been increasing due to the rising health and safety awareness of the global community. In view of this, fully integrated, high speed, and portable deoxyribonucleic acid (DNA) analyzers are urgently needed. One of the key challenges is the fluidic control without requiring any external bulky pump. This study aims to develop a continuous-flow polymerase chain reaction (CFPCR) microchip with integrated on-chip electrolytic pump. In this chapter, the background information of the study is presented in Section 1.1, a comprehensive literature review is provided in Section 1.2, and the objectives of this study are stated in Section 1.3.

1.1 Background

Over the past few decades, the utilization of microelectromechanical systems (MEMS) has grown rapidly in numerous fields such as automotive industry, microelectronics, and telecommunications. Recently, the development of 'BioMEMS', MEMS technologies for biological uses, has become a popular research topic [1]. The applications of BioMEMS improve the conditions of many biological practices due to its remarkable characteristics including high speed analysis, low consumption of samples and reagent, as well as high throughput and portability.

DNA analysis is one of the interesting fields in BioMEMS. It is important for many applications such as medical diagnosis, environmental/food pathogen detection, and forensic analysis. It consists of three main steps: sample preparation, amplification (e.g., polymerase chain reaction (PCR)), and detection. Typically, these steps are performed by using bulky and high-cost machines in a well-equipped laboratory. However, due to the mounting need for point-of-care testing and on-site detection, the development of fully integrated portable DNA analysis system becomes essential.

One of the key steps for DNA analysis is PCR. The amount of DNA molecules in a sample is usually not sufficient for direct detection. Therefore, PCR is used to amplify the minute amount of specific DNA sequence into large quantity prior to detection. However, conventional PCR is carried out with bulky benchtop instrument, which hinders the development of a portable DNA analysis system. In the next section, a literature review is provided to introduce different aspects related to microchip-based PCR.

1.2 Literature Review

In this literature review, a brief introduction of PCR is given in Section 1.2.1. This is followed by a detailed summary of various types of microchip-based PCR in Section 1.2.2. Then, surface passivation for microchip-based PCR is introduced in Section 1.2.3. Finally, microfluidic control is discussed in Section 1.2.4, with particular focus on on-chip micropumps.

1.2.1 Polymerase Chain Reaction

PCR is an important molecular biology technique to amplify DNA exponentially. It was first introduced in 1986 by Kary Mullis [2]. The reaction involves thermal cycling at three temperatures of denaturation (95 °C), primer annealing (50–55 °C), and extension (70–75 °C), as shown in Figure 1.1. In denaturation, a double-stranded DNA molecule is separated into two single-stranded DNA molecules. In primer annealing, a pair of primers, which are short oligonucleotides, bind to a specific region of a DNA template in a complementary manner (i.e., A–T and C–G base-pairing) to define the amplification region. In extension, nucleotides are added one-by-one by Taq DNA polymerase to extend the hybridized primer. After one thermal cycle, the number of specific DNA sequence is doubled. Therefore, one single DNA molecule can theoretically be duplicated to 2^{30} copies (i.e., one billion copies) after 30 thermal cycles. Normally, conventional PCR thermal cycler takes about 1–2 h to complete 30 cycles of PCR.

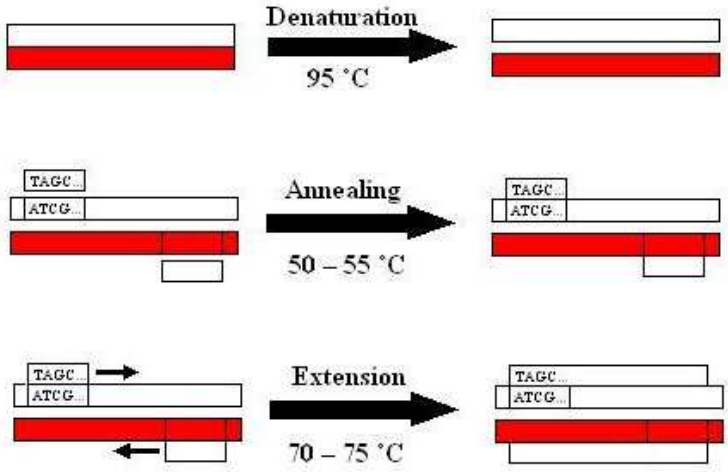

Figure 1.1 A schematic diagram of PCR showing the three key temperature steps.

1.2.2 Microchip-Based PCR

In recent years, there have been many researches on microchip-based PCR due to its benefits of low consumption of reagents/samples, short analysis time, high-throughput, and small size. Generally, microchip-based PCR can be classified into stationary and continuous-flow types [3-4].

The stationary PCR involves thermal cycling inside a reaction chamber. The speed of the stationary PCR depends to a great extent on the heating and cooling rates. With MEMS technology, the size and thermal mass of the device are greatly reduced, thereby improving the temperature cycling rate and thus the overall reaction time is significantly reduced. In 1993, a stationary PCR microchip was first introduced by Northrup and co-workers, as shown in Figure 1.2 [5]. Polysilicon heaters were patterned under a silicon reaction chamber for thermal cycling. However, the repeating heating and cooling processes in each cycle took up a significant fraction of the total amplification time.

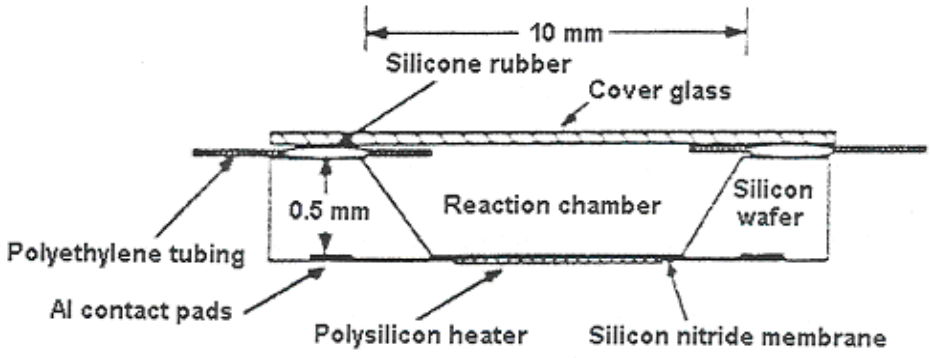

Figure 1.2 A cross-sectional view of the stationary microchip-based PCR developed by Northrup *et al.* in 1993.

To improve the throughput of PCR microchip, Poser *et al.* developed a device which could perform more than one PCR at the same time by using multi-chamber stationary PCR microchip. A sketch of their design is shown in Figure 1.3 [6].

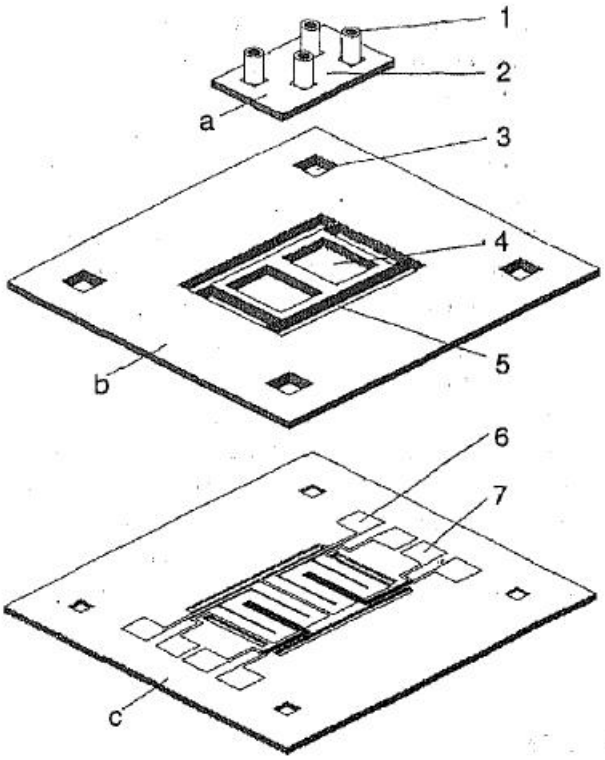

Figure 1.3 A sketch of two-chamber PCR microchip developed by Poser *et al*. The microchip consisted of 3 layers: a) cover; b) topside; c) backside; and 7 components: 1) inlet; 2) cover; 3) adjustment; 4) reaction chamber; 5) air chamber; 6) thin-film heater; 7) temperature sensor.

Since then, many research efforts have focused on temperature control [7-12], surface treatment [13-14], fluidic flow [15-18], real-time detection [19-20], multiplex PCR [21], and integration with other steps in DNA analysis [22]. In 2004, Liu *et al.* developed a fully integrated microchip to perform DNA analysis (Figure

1.4) [23]. Sample preparation, DNA amplification in a stationary chamber, and detection were all included in a single microchip. The flow of reagents in the microchip was regulated by microvalves and micropumps. The micropumps included thermopneumatic and electrochemical pumps. However, the whole analysis process was time consuming. The time required for sample preparation, DNA amplification, DNA hybridization, and fluidic control were 50, 90, 60, and 10 min, respectively.

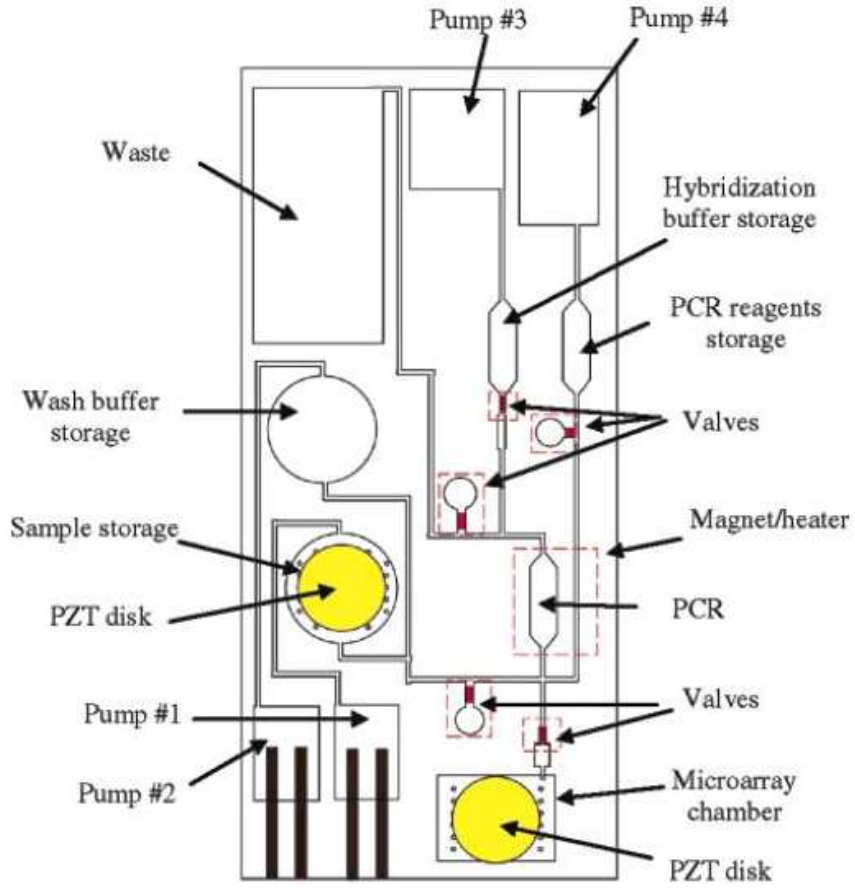

Figure 1.4 A schematic diagram for the plastic fluidic chip developed by Liu *et al* [23].

CFPCR microchips can be classified into unidirectional, rotary closed-loop, and oscillatory types. The comparison of CFPCR microchips is provided in Table 1.1. In 1998, the first CFPCR microchip was developed by Kopp *et al.*, as shown in Figure 1.5 [24]. Instead of changing the temperature of the reaction chamber, PCR solution was repeatedly transported through three temperature regions in a unidirectional microfluidic channel for thermal cycling. This type of PCR addressed the problem of low heating and cooling rates of the stationary PCR. The theoretical time for achieving thermal equilibrium was less than 100 ms for Kopp's design. The total amplification time was controlled by the sample flow rate and dimensions of the microchannel, which could be adjusted easily.

Table 1.1 Comparisons of CFPCR microchip.

Pumping method	Duration (min)	PCR cycle	Base pair	Type of target	Type of CFPCR microchip	References
Syringe pump	10	40	392	dna	unidirectional	25
Thermal gradient	100	35	112	dna	closed-loop	26
Syringe pump	13.4	40	99	dna	unidirectional	27
NA	NA	NA	120	rna	unidirectional	28
Syringe pump	92	35	143	rna	unidirectional	29
Syringe pump	93	40	143	rna	unidirectional	30
Syringe pump	34	42	292	dna	unidirectional	31
Syringe pump	8.5	33	323	dna	unidirectional	32
Syringe pump	11	35	180	dna	unidirectional	33
Syringe pump	23	30	79	dna	unidirectional	34
Syringe pump	30	40	418	dna	unidirectional	35
Syringe pump	47	30	240	dna	unidirectional	36
Syringe pump	70	35	572	dna	unidirectional	37
Syringe pump	70	35	572	dna	unidirectional	38
Syringe pump	10-15	33	249	dna	unidirectional	39
Syringe pump	9-45	40	392	dna	unidirectional	40

Syringe pump	8.5-34	26	500	dna	unidirectional	41
Syringe pump	8-30	30	430	dna	unidirectional	42
Pneumatic micropump	100	45	350	dna	closed-loop	43
Syringe pump	NA	30	450	dna	unidirectional	44
Syringe pump	9	40	230	dna	unidirectional	45
Syringe pump	59.5	40	NA	dna	unidirectional	46
NA	NA	25	NA	dna	unidirectional	47
Thermal gradient	8.16	20	99	dna	closed-loop	48
Syringe pump	23	30	298	dna	unidirectional	49
Syringe pump	17-52	30	298	dna	unidirectional	50
Syringe pump	18.7	30	200	dna	unidirectional	51
NA	35-40	31	230	dna	unidirectional	52
Syringe pump	12	40	287	dna	oscillation	53
Magnetohydrodynamic force	NA	20	142	dna	closed-loop	54
Capillary force	23	30	500	dna	closed-loop	55
Syringe pump	12-18	30	230	dna	unidirectional	56
Micro peristaltic pump	NA	NA	NA	dna	oscillation	57
Syringe pump	60	30	1460	dna	unidirectional	58
Micro Injector	13	35	NA	dna	oscillation	59
Thermal gradient	73	35	700	dna	closed-loop	60
Thermal gradient	NA	NA	295	dna	closed-loop	61
Rotary pump	30	30	199	dna	closed-loop	62
Syringe pump	35	25	150	dna	closed-loop	63
Syringe pump	NA	20	90	dna	unidirectional	64
Syringe pump	18.7	20	176	dna	unidirectional	24
Syringe pump	17	34	85	dna	unidirectional	66
Syringe pump	11	30	181	dna	unidirectional	67
Syringe pump	2.3-24	15	120	dna	unidirectional	68
Syringe pump	1.7-3	20	500	dna	unidirectional	69
Syringe pump	40	26	489	dna	unidirectional	70
Vapor pressure	2	40	134	dna	unidirectional	71
Syringe pump	40	50	113	dna	unidirectional	72
Syringe pump	14.6	20	>600	dna	unidirectional	73
Electrokinetical force	18.1	27	500	dna	closed-loop	74
Syringe pump	9-70	20	300	dna	unidirectional	75
NA	NA	20	NA	dna	unidirectional	76
Magnetic force	40	25	247	dna	closed-loop	77

Syringe pump	38	30	240	dna	oscillation	78
Syringe pump	30	25	450	dna	unidirectional	79
Syringe pump	10	30	134	dna	unidirectional	80
Syringe pump	NA	20	500	dna	oscillation	81
Syringe pump	35	35	278	dna	oscillation	82

* NA = not available

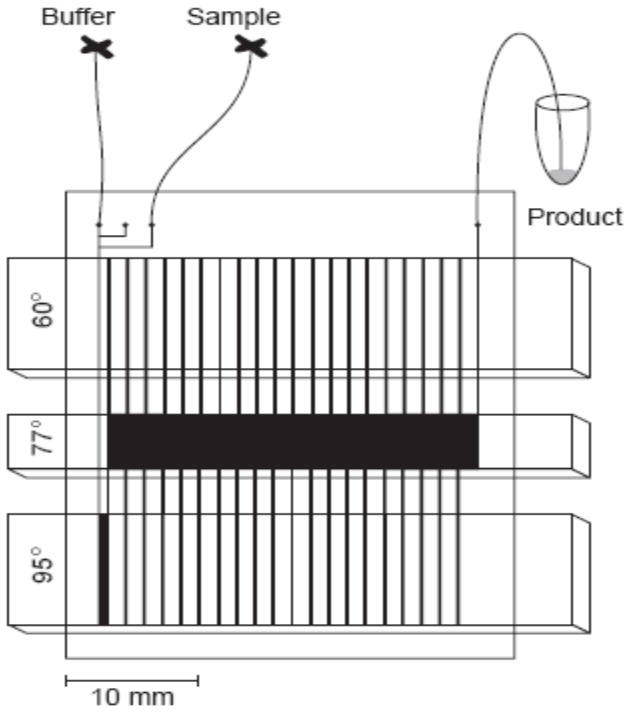

Figure 1.5 A continuous-flow PCR in glass chip developed by Kopp *et al.* in 1998.

Kopp *et al.* successfully amplified the target gene in less than 19 min with an observable PCR product band in gel electrophoresis, as shown in Figure 1.6. The amplification efficiency was comparable to the commercial thermal cycler. The main limitation of the unidirectional CFPCR is the difficulty in adjusting the number of thermal cycles [25].

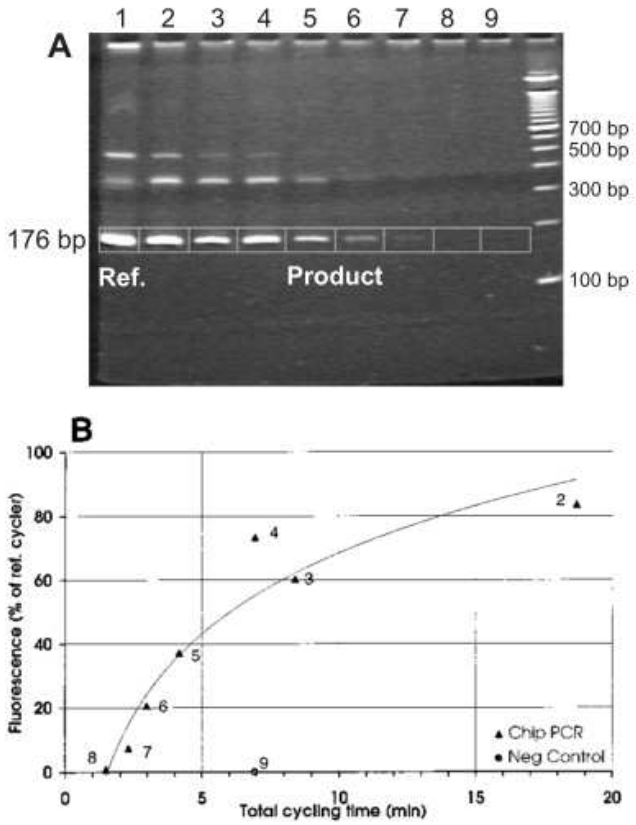

Figure 1.6 (A) Gel electrophoresis results of the CFPCR by Kopp *et al.* Lane 1 is the control with conventional thermal cycler; lanes 2 to 8 are the CFPCR with decreasing thermal cycling duration from 18.8 to 1.5 min. (B) Fluorescence signals of the CFPCR products against thermal cycling duration.

In 2002, Liu *et al.* developed a rotary closed-loop CFPCR [62], as shown in Figure 1.7. In their design, PCR reagent was repeatedly circulated through a circular closed microchannel by pneumatically controlled on-chip valves with peristaltic pumping capability. The closed-loop CFPCR allows the adjustment of the number of thermal cycles. However, its main limitation is the bulky off-chip pumping system.

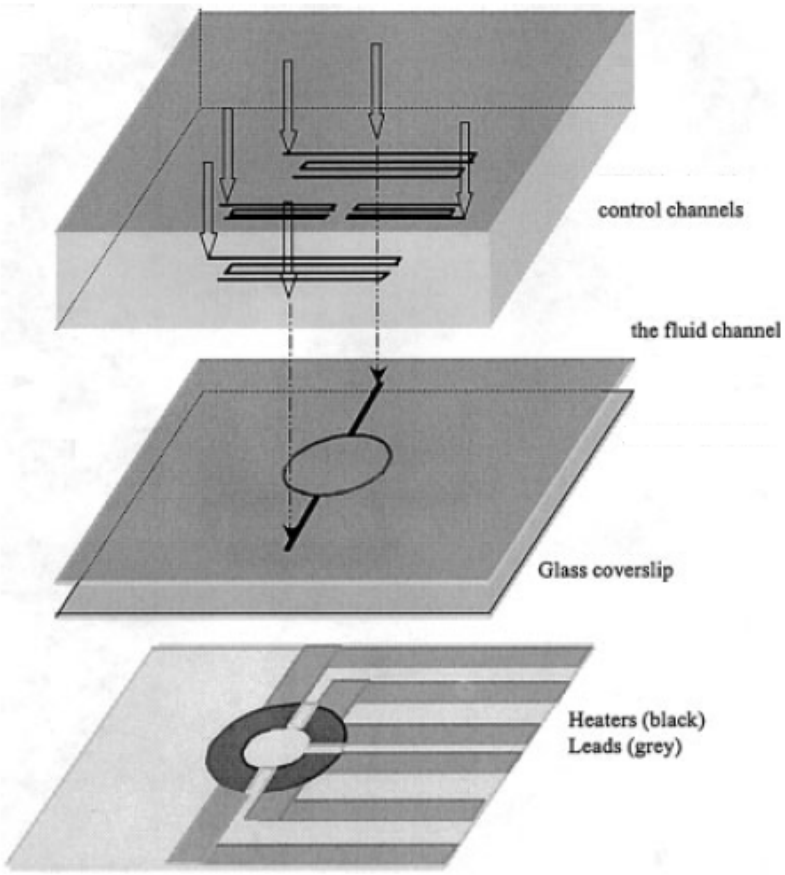

Figure 1.7 Assembly of the closed-loop CFPCR by Liu *et al*. Block with control channels at the bottom surface (top layer), thin layer with fluid channel at the bottom surface and glass coverslip (middle layer), and heaters with leads on a glass substrate (bottom layer). Arrows indicate the air and fluid through-holes [62].

An oscillatory CFPCR was developed by Wang *et al.* in 2005, as shown in Figure 1.8 [59]. Their design consisted of only one straight microchannel with three independent temperature zones for thermal cycling. The PCR process was performed by driving PCR reagent back and forth through the microchannel. The oscillatory CFPCR allows the adjustment of the number of thermal cycles. However, external pump is needed.

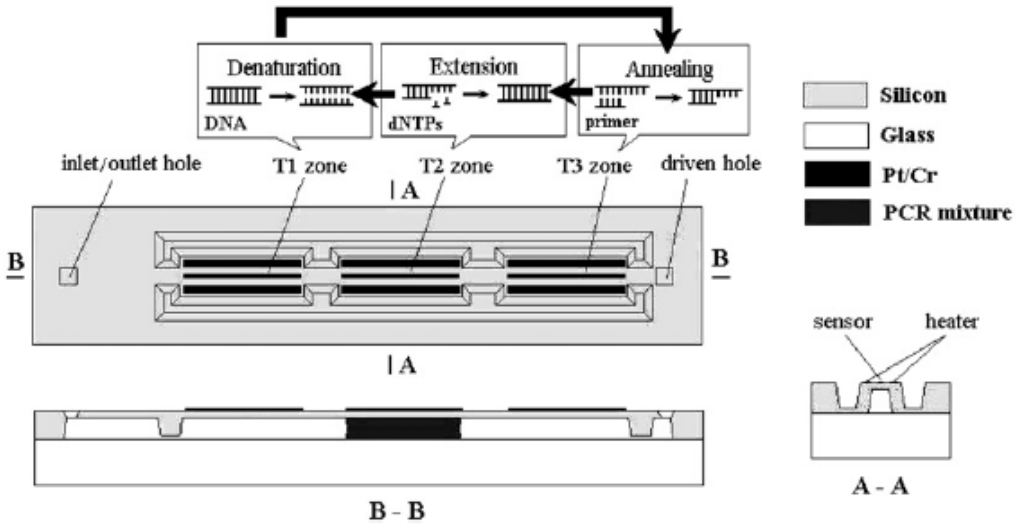

Figure 1.8 A schematic structure of the oscillatory CFPCR by Wang *et al*.

Hashimoto *et al.* investigated the effect of flow velocity on amplification efficiency of CFPCR [68]. In their experiments, 500- and 997-base-pair (bp) DNA were amplified in 1.7 min (5.2 s/cycle) and 3.2 min (9.7 s/cycle) for 20 cycles, respectively. The amplification time of CFPCR was limited by the enzyme kinetics of Taq DNA polymerase (i.e., extension step with a rate of 1,000 bp/min). The amplification signal was observed at cycle rate as low as 5.2 s/cycle, as shown in Figure 1.9.

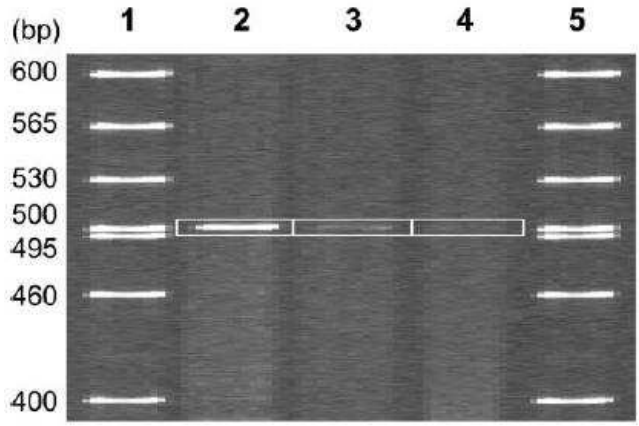

Figure 1.9 Effect of linear velocity on the generation of a 500-bp PCR product from Hashimoto *et al*. Lanes 1 and 5 are DNA size markers; lanes 2–4 are the CFPCR products at cycle rates of 7.8, 5.2, and 3.9 s/cycle, respectively.

The short amplification time of CFPCR has attracted considerable attention to further develop this system. Researches have focused on the thermal control [28, 44, 66, 68, 83, 84], real-time detection [69], fabrication and materials [39, 41, 42, 46, 67, 75, 85-88], fluidic control [61, 64, 89-93], integration with other steps in DNA analysis [94], and parallel processing [95]. Nevertheless, the utilization of bulky equipment such as syringe pump would reduce the portability of the device. An example of a continuous-flow reverse transcription-PCR is shown in Figure 1.10 [94].

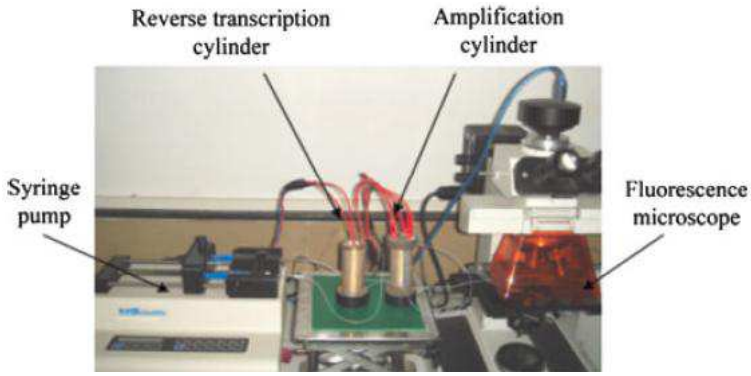

Figure 1.10 Photograph of the setup for a continuous-flow reverse transcription-PCR system with fluorescence detection [94].

1.2.3 Surface Passivation

Biocompatibility is one of the most important issues for successful DNA amplification in PCR microchip. Due to the high surface area to volume ratio, the surface property of the microchip has significant influence on the amplification efficiency. Wilding *et al.* showed that the PCR amplification efficiency in a bare silicon microchip was lower than that in the conventional thermal cycler, as shown in Figure 1.11 [96].

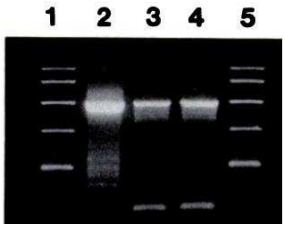

Figure 1.11 Gel electrophoresis image of PCR results from Wilding *et al.* Lanes 1 and 5 are DNA size marker; lane 2 is PCR performed by thermal cycler; lanes 3 and 4 are PCR performed by microchip.

Erill *et al*. conducted a study to investigate the inhibition arising from the non-specific adsorption of Taq DNA polymerase onto surfaces in glass–silicon PCR microchips. As shown in Figure 1.12, their results suggested that the inhibition effect in microchips was dependent on both the surface material(s) and area [97].

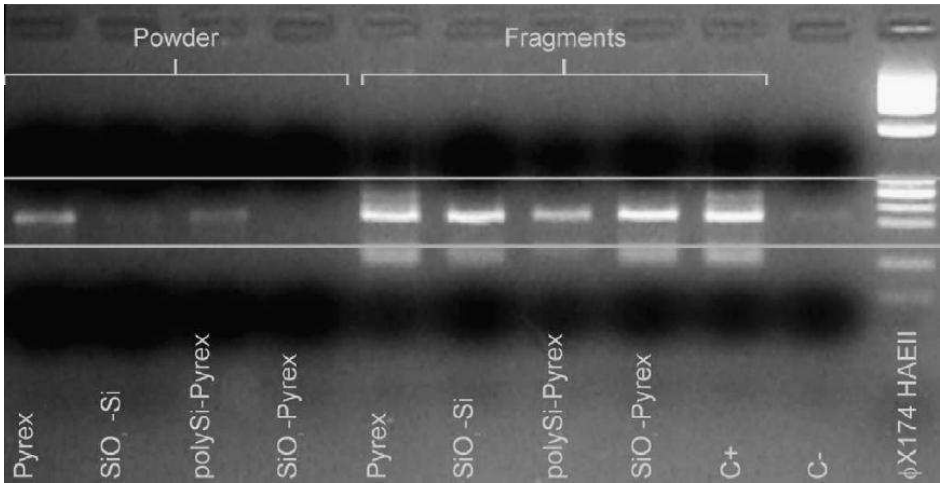

Figure 1.12 Gel electrophoresis results showing the effects of material and surface area on PCR inhibition by Erill *et al* [97].

Prakash *et al.* studied the adsorption of Taq DNA polymerase on various materials which were commonly applied in microfluidics [98]. Contact angle measurement was used to investigate the adsorption behavior (Table 1.2). Materials such as glass and SU8 had contact angles < 30° after 600-s incubation with Taq DNA polymerase and continued to recede (termed as propagating adsorption materials), whereas materials such as polytetrafluoroethylene (Teflon) and polydimethylsiloxane (PDMS) had contact angles > 40° after 600-s incubation and did not recede further (termed as contained adsorption materials).

Table 1.2 Taq DNA polymerase adsorption in various materials using contact angle measurement.

Material	Supplier	Contact angle (CA) of sessile droplet			Implied material classification[a]
		DI-H_2O (time invariant)	*Taq* (enzyme)		
			t = 5 s	t = 600 s	
Glass	Corning, USA	25°	14°	<8°	Propagating adsorption
Polyethylene glycol (PEG)	J.T. Bakar, USA	35°	25°	<10°	Propagating adsorption
Polymethyl methacrylate (PMMA)	MicroChem, USA	60°	45°	<10°	Propagating adsorption
Poly(vinylidene chloride) (PVDC)	S.C. Johnson, Canada	95°	45°	<20°	Propagating adsorption
Trimethylchrolosilane (SafetyCoat™)	J.T. Baker, USA	95°	52°	<30°	Propagating adsorption
Polyamide	DuPont, USA	55°	55°	<8°	Propagating adsorption
HPR 504	Shiply, USA	60°	58°	<10°	Propagating adsorption
SU8 (2000.5)	MicroChem, USA	60°	60°	<10°	Propagating adsorption
Polyethylene film (PE)	Glad Metric, Canada	65°	60°	<10°	Propagating adsorption
Mincor® S 300	BASF, Germany	165°	115°	<10°	Propagating adsorption
Teflon® AF (polytetrafluoroethylene)	DuPont, USA	110°	60°	58°	Contained adsorption
ParaFilm® Wax film	Ameri. Natl. Can™, USA	115°	46°	43°	Contained adsorption
Poly dimethylsiloxane (PDMS)	Dow Corning, USA	90°	75°	40°	Contained adsorption

[a] Materials on which the contact angle recedes (<30° after 600 s and continues to recede) due to *Taq* (enzyme) adsorption are classified as "*propagating* adsorption" materials, while those with static droplet contact angle (>40° after 600 s and remains time-invariant) are classified "*contained* adsorption" materials. [CA error ±2°]

To reduce PCR inhibition by the surface material of microchip, surface passivation is applied to minimize the interaction between the surface and PCR reagents. Generally, the passivation can be classified into static and dynamic types. Static passivation involves pre-coating the inner surface of microchip with PCR-friendly chemical before performing PCR [4]. For example, Rodriguez *et al.* placed bovine serum albumin (BSA) solution in a microchip's reaction chamber for 2 to 3 min to perform the static passivation [99]. Shoffner *et al.* treated a microchip's reaction chamber with a silanizing agent for 15 min, followed by incubation of polymer solutions such as polyadenylic acid and polyvinylpyrrolidone (PVP) for 1 h [100]. Dynamic passivation involves the addition of a passivating agent to PCR mixture such BSA, PVP, and polyethylene glycol (PEG). Friedman and Meldrum used BSA to prevent Taq DNA polymerase from adsorbing onto microchip's reaction chamber surface [101]. Xia *et al.* minimized the surface effect of PDMS–glass microchip on PCR by using PEG and PVP [102].

1.2.4 Microfluidic Control

One important aspect of CFPCR is fluidic control. An external syringe pump is commonly used for this purpose. However, this makes the overall size of the system too large for portable applications. Alternatively, an on-chip micropump can be used to achieve an integrated and self-contained device. Micropumps can be classified into mechanical and non-mechanical types with different actuation methods, as shown in Figure 1.13 [103].

The mechanical micropumps usually involve periodic movement of diaphragms to drive fluids by different actuation methods such as electrostatic, piezoelectric, and thermopneuamtic forces. Different mechanical micropumps were integrated to the stationary PCR microchips for fluidic control, which are summarized in Table 1.3 [15]. However, the fabrication of these micropumps is complicated, which is not conducive to their widespread use [57, 104, 105].

The non-mechanical micropumps involve the conversion of non-mechanical energy to kinetic energy for driving fluid flow (Table 1.4 [103]). In contrast to mechanical micropumps, non-mechanical pumps are relatively simple in design and fabrication [103]. The power consumption is another important consideration. Electroosmotic and electrohydrodynamic micropumps have high power consumption. In 2004, Chen *et al.* developed electrokinetic micropumps for CFPCR chips with adjustable cycle number, as illustrated in Figure 1.14. However, the required voltage is very high which is not suitable for portable device [73]. On the other hand, electrolytic micropump has much lower power consumption.

Electrolytic pump is based on the electrolysis of water. Chemical reactions are driven by external voltage or current source, leading to the generation of gas bubbles based on the following two half-cell reactions:

Anode: $2\ H_2O \rightarrow 4\ H^+ + 4\ e^- + O_2\,(g)$ (1)

Cathode: $2\ H_2O + 2\ e^- \rightarrow 2\ OH^- + H_2\,(g)$ (2)

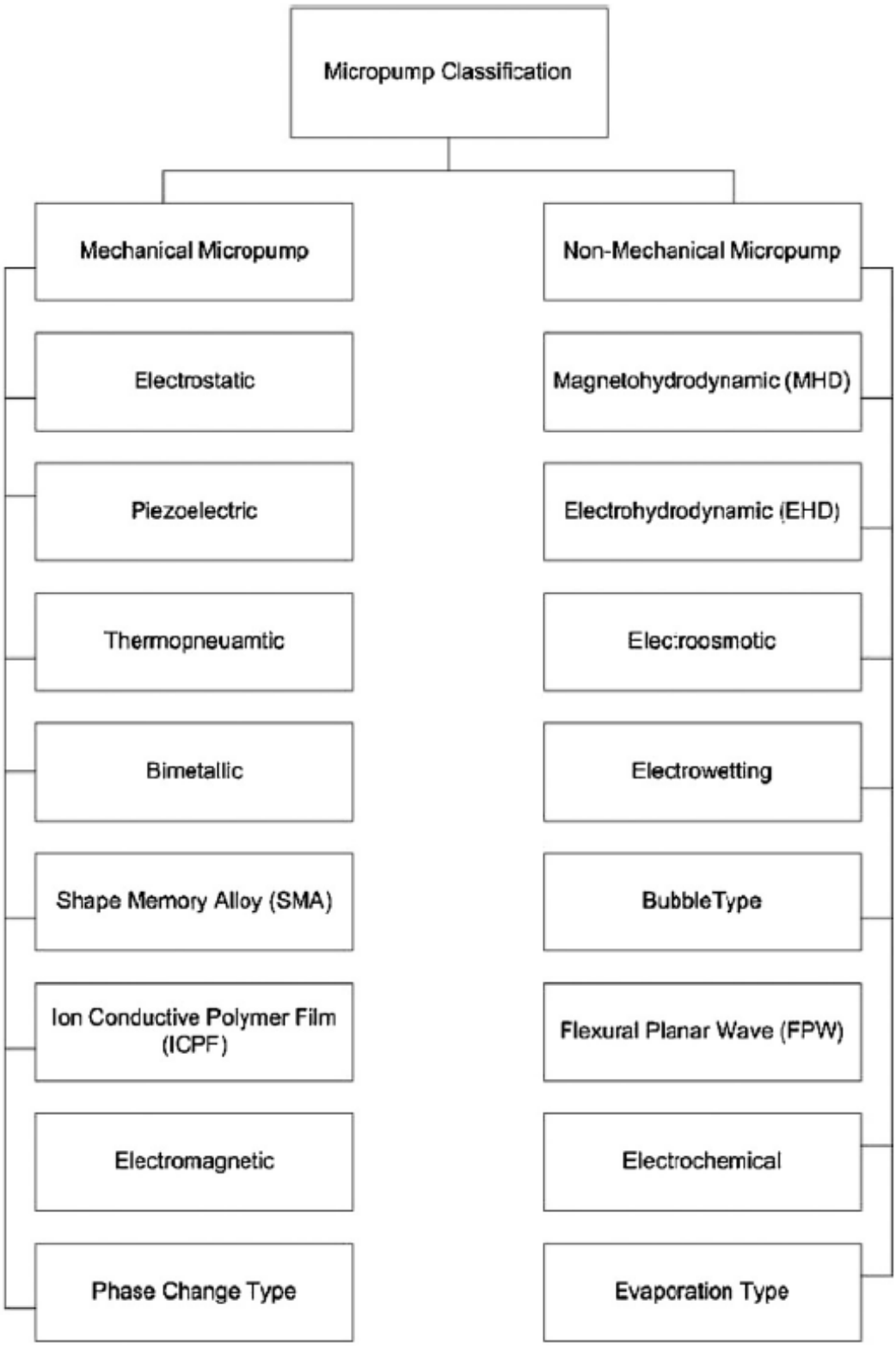

Figure 1.13 Micropumps with different actuation methods.

Table 1.3 Mechanical micropumps for PCR microchips.

Reference	Driver	Check valves	Construction	Pump chamber	Diaphragm material	Diaphragm thickness (mm)	V (V)	f (Hz)	Δp_{max} (kPa)	Q_{max} (mL s^{-1})
Bu et al. (2003)	Piezoelectric (axial)	None	Glass-silicon	3 (S)	Glass	0.2	100	10	50-60	3.14
Liao et al. (2005)	Pneumatic	None	PDMS-glass	3(S)	PDMS		9	15	69	0.0667
Lien et al. (2007)	Pneumatic	None	PDMS-PDMS-glass	3(S)	PDMS	0.3		11	173	1.67
Huang et al. (2006)	Pneumatic	None	PDMS-PDMS-glass-PMMA	3(S)	PDMS			~15	138	~0.1
(Chou et al., 2001; Liu et al., 2002a, 2003a)	Pneumatic	None	Multi-layer elastomer (PDMS)	6 (S)	Elastomer PDMS					
Easley et al. (2006)	Pneumatic	Flap (diaphragm)	Glass-PDMS-glass-glass	1	PDMS	0.254	12	5–7	60	0.0644
(Pilarski et al., 2005; Prakash et al., 2005; Kaigala et al., 2006)	Electric-servomotor	None	PDMS-glass	3(S)	PDMS	~1				

Note: S — series configuration; V — micropump operating voltage; f — micropump operating frequency; Δp_{max} — maximum measured micropump differential pressure; Q_{max} — maximum measured volumetric flow rate.

Table 1.4 Non-mechanical micropumps.

Actuation mechanism	Reference	Fabricated structure	Size (mm)	Voltage (V)	Pressure (kPa)	Flow rate (μl/min)	Pumping medium	Application reported in reference
MHD-DC type	Jang and Lee [81]	Si–Si	n/r	60	0.17	63	Seawater	n/r
	Huang et al. [82]	PMMA	n/r	15	n/r	1200	n/r	Drug delivery, biomedical studies
MHD-AC type	Heng et al. [83]	Glass-PMMA	n/r	15	n/r	1900	n/r	n/r
	Lemoff and Lee [85]	Glass-Si-glass	n/r	n/a	0	18	NaCl solution	n/r
EHD	Ritcher and Sandmaier [86]	Si–Si	3 mm × 3 mm	600	0.43	14000	Ethanol	n/r
	Fuhr et al. [87]	Si-glass	n/r	40	n/r	2	Water	n/r
	Darabi et al. [88]	Ceramic	638.4 mm^3	250	0.78	n/r	3MHFE-7100	n/r
Electroosmotic	Zeng et al. [91]	Packed silica particles	85 mm^3	2000	2000	3.6	Water	n/r
	Chen and Santiago [92]	Soda–lime glass	9000 mm^3	1000	33	15	Water	n/r
	Takemori et al. [94]	Si-plastic	n/r	2000	10	0.1	Degassed 50 mm Trisborate buffer (pH 9.3)	n/r
	Wang et al. [95]	Fused silica-glass	n/r	6000	25	2.6	Water	Micro-analysis systems
Electrowetting	Yun et al. [96]	Glass-SU8-Si-Si	n/r	2.3	0.7	170	Water	n/r
Bubble type	Tsai and Lin [97]	Glass-Si	n/r	20	0.38	4.5	Isopropyl alcohol	n/r
	Zahn et al. [99]	SOI-quartz dice	n/r	n/r	3.9	0.12	Water	Continuous monitoring DDS/ monitor glucose levels fro diabetes patients
FPW	Luginbuhl et al. [103].	Silicon-platinum-sol–gel-derived piezoelectric ceramic	n/r	n/r	n/r	0.255	Water	n/r
	Nguyen et al. [104]	Aluminum, piezoelectric zinc oxide, silicon nitride	n/r	n/r	n/r	n/r	Water	μTAS, cell manipulating systems, and drug delivery systems.
Electrochemical	Suzuki and Yoneyama [107]	Glass-Si	n/r	n/r	n/r	n/r	Standard solution of CuSO4	Drug delivery
	Yoshimi et al. [108]	Glass-platinum electrode	n/r	3	n/r	n/r	Neurotransmitter solution	Administration of neurotransmitters to neurons. Create Synapses in artificial sensory organs.
	Kabata and Suzuki [109]	Glass-platinum electrode-polyimide	n/r	1.4	n/r	13.8	Insulin	Injection of insulin and monitoring of glucose concentration
Evaporation based	Effenhauser et al. [110]	Plexiglass	n/r	n/r	n/r	0.35	Ringers solution	Continuous monitoring DDS/continuous glucose monitoring for diabetes patients

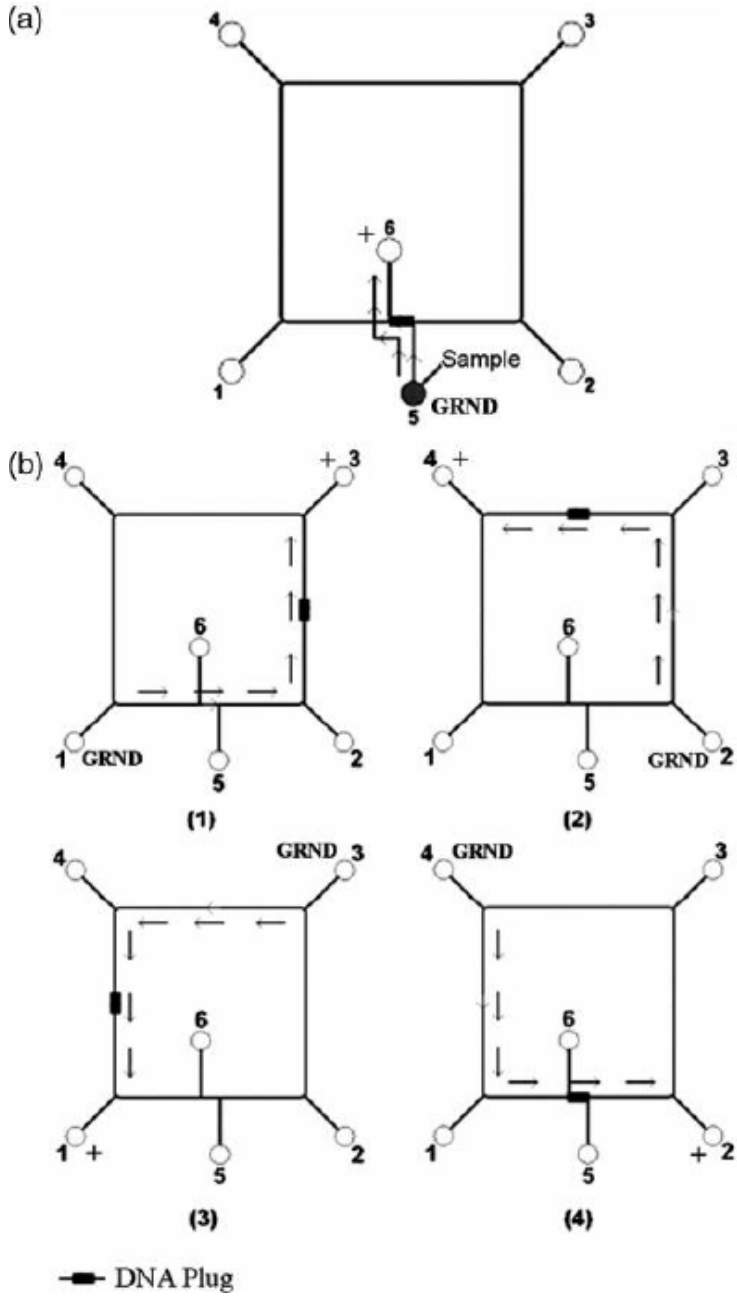

Figure 1.14 Schematic diagram showing the principle of electrokinetic synchronized cyclic continuous-flow PCR process by Chen *et al*. (a) Sample was filled into reservoir 5, and 800 V was applied to the electrodes in reservoirs 5 and 6. (b) One cycle included four steps. The DNA plug was driven when the 1.5 kV was applied to different pairs of electrodes.

By adjusting the voltage or current applied to the electrodes, the volume of gas bubbles generated can be controlled. Under isobaric conditions, the theoretical maximum strain and stress that can be achieved are about 136,000% and 200 MPa, respectively [106].

Electrolytic micropumps with different designs had been developed [107-114], which were applied to many applications such as dosing systems and drug delivery applications. Böhm *et al*. developed a micromachined electrochemical pump for dosing precise amount of liquid [115]. In their design, oxygen and hydrogen gases were generated by applying positive and negative pulses sequentially to platinum (Pt) electrodes. The volume of gas produced was given by the following equation:

$$\Delta V = \frac{3i(\Delta t_1 - \Delta t_2)}{4F} V_m \tag{3}$$

where ΔV = volume of gas produced, i = current, Δt_1 = duration of the positive pulse, Δt_2 = duration of the negative pulse, F = Faraday's constant (96,485 $Cmol^{-1}$), and V_m = molar gas volume (24 dm^3mol^{-1}). Böhm *et al.* further developed the electrochemical micropump into a closed-loop control system [116]. The cell impedance of the reservoir was used to control the applied current for the actuation of the micropump.

Li *et al.* designed a drug delivery device for the treatment of incurable ocular diseases [117], as shown in Figure 1.15. The device consisted of interdigitated Pt electrodes, which were patterned on an oxidized silicon substrate. Gas bubbles were generated by the electrolysis of water and acted as the actuation force.

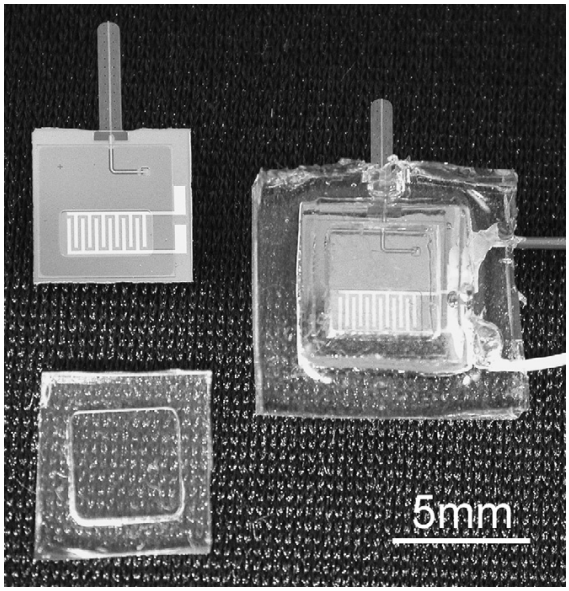

Figure 1.15 An electrolytically actuated drug delivery device by Li *et al*.

Another concern for microfluidic control in CFPCR is the formation of bubbles due to the high temperature in the denaturation zone. The presence of bubbles in a microchannel causes irregular and unstable flow of PCR mixture, and thus the amplification efficiency is reduced. In 2006, Nakayama *et al.* prevented bubbles generation by introducing fluorinated oil in front of PCR mixture to increase the internal pressure of the flowing stream, as shown in Figure 1.16 [71, 118]. Wu *et al.* suggested the introduction of highly viscous paraffin oil plugs at both the anterior and posterior ends of an ink sample, as shown in Figure 1.17. In addition, the theoretical basis for bubbles formation and elimination was provided [119].

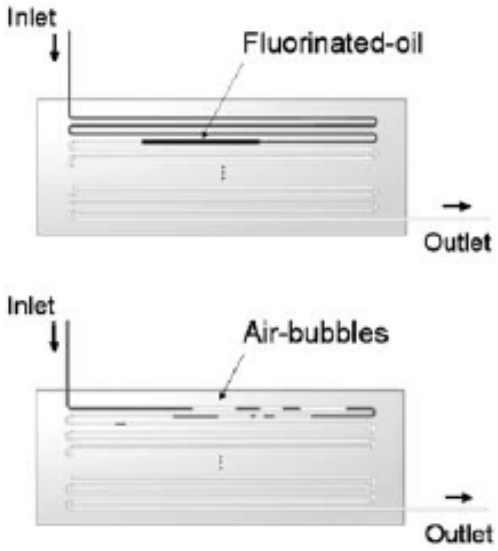

Figure 1.16 Schematic illustration showing the flow (top) with PCR reagents and fluorinated oil and (bottom) with PCR reagents only.

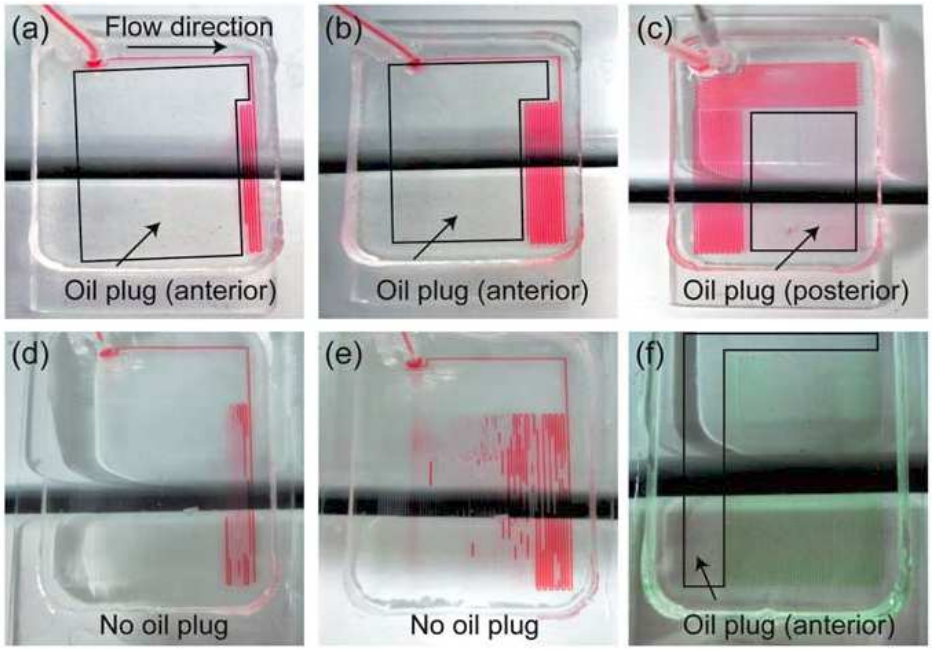

Figure 1.17 (a–c) Bubble elimination with paraffin oil plugs at both the anterior and posterior ends of the ink plug. (d–e) Bubble was generated without the paraffin oil plugs. (f) PCR sample with the paraffin oil plugs.

1.3 Objectives

PCR has been widely used in DNA analysis for numerous applications such as medical diagnostics, food and water monitoring, and biological warfare defense. Nonetheless, portable DNA analysis systems for point-of-care or on-site DNA testing are still rare in the market. One of the main reasons is the use of stationary PCR, which has long operation time due to the heating and cooling processes. On the other hand, CFPCR, which does not require repeated heating and cooling processes, enables ultra-fast DNA amplification. Syringe pump is commonly used to drive PCR mixture through a microchannel in CFPCR chip. However, it is difficult to integrate the bulky syringe pump into a portable device. Toward a self-contained CFPCR microchip, a small size, low power consumption, and easy-to-fabricate micropump should be chosen. In this study, the goal is to develop a portable microchip-based CFPCR device with on-chip electrolytic micropump. The effects of applied voltage of the electrolytic micropump on amplification time and efficiency are studied. In addition, the effects of the presence of a silicone oil plug, concentration of Taq DNA polymerase, and dynamic/static passivation with BSA on amplification efficiency are studied.

CHAPTER 2

METHODOLOGY

The design and fabrication of the CFPCR device with on-chip electrolytic pump will be presented in this section. The device consists of three main components: CFPCR microchip, electrolytic pump microchip, and temperature control system (Figure 2.1). The design and fabrication of the CFPCR and electrolytic pump microchips are discussed in Section 2.1 and Section 2.2, respectively. The bonding of the CFPCR microchip with the electrolytic pump substrate is presented in Section 2.3. The design and fabrication of the temperature control system are discussed in Section 2.4. Finally, the PCR experiments are detailed in Section 2.5.

2.1 CFPCR Microchip

In this section, the design of the CFPCR microchip is given in Section 2.1.1. This is followed by the fabrication procedures in Section 2.1.2.

2.1.1 Design of CFPCR Microchip

The fluid storage, partitioning, and guidance are the main design considerations for the CFPCR microchip. It consists of four main regions: pumping chamber, PCR reservoir, oil reservoir, and PCR region, as shown in Figure 2.2. The dimensions of the design are detailed in Figure 2.3.

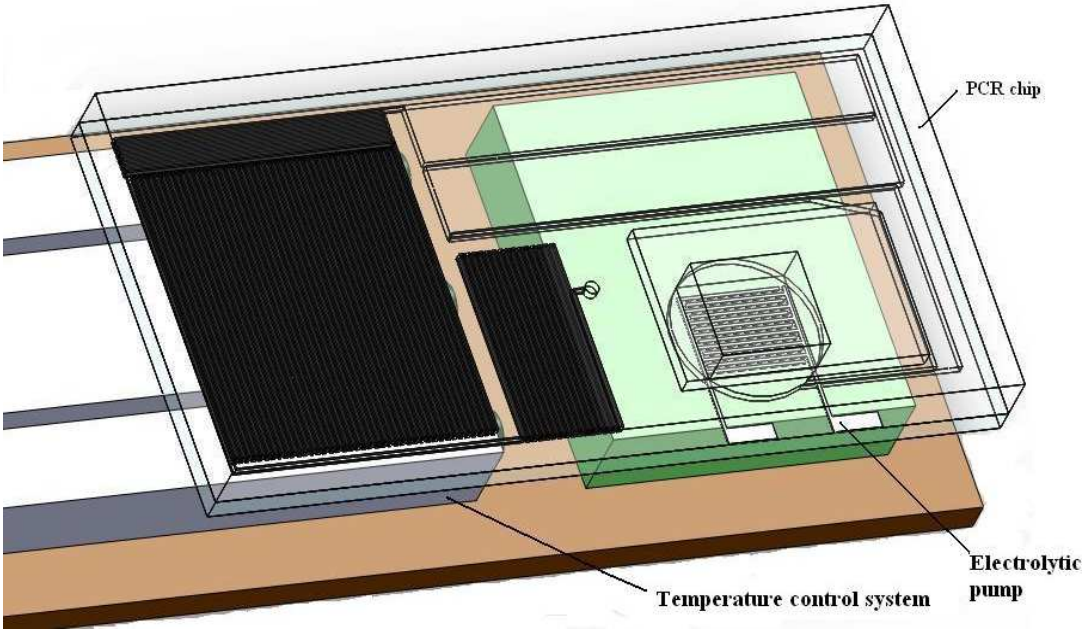

Figure 2.1 A CFPCR device consisting of CFPCR microchip (top layer), electrolytic pump microchip (middle layer), and temperature control system (bottom).

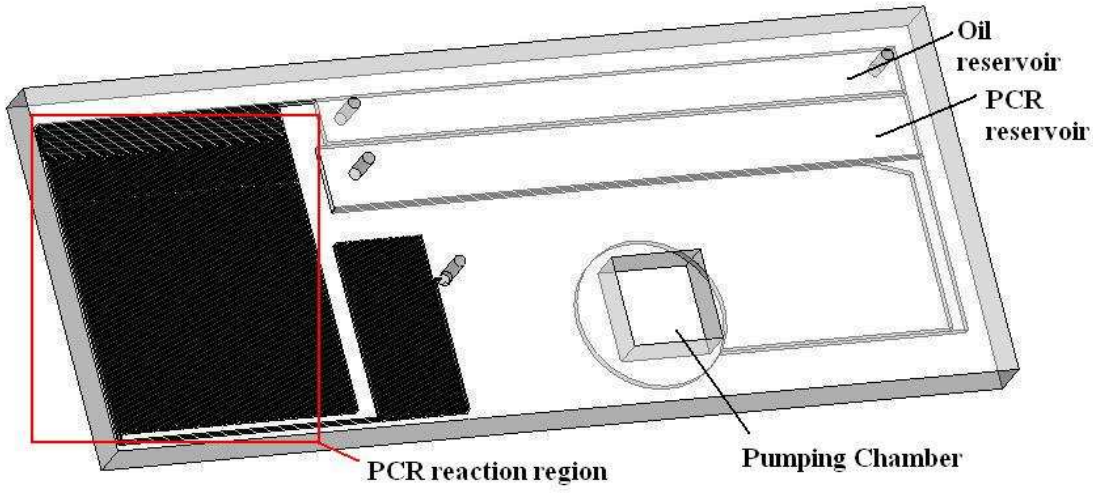

Figure 2.2 A CFPCR microchip consisting of four main regions: pumping chamber, PCR reservoir, oil reservoir, and PCR region.

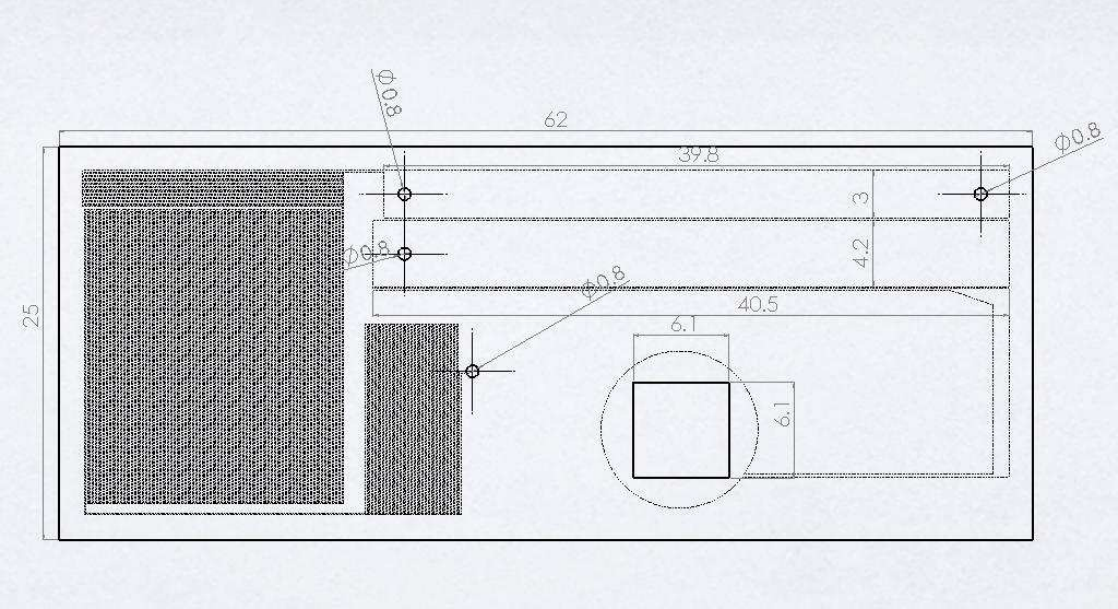

Figure 2.3 Detailed dimensions (expressed in mm) of the CFPCR microchip.

The pumping chamber acts as a reservoir for containing an electrolyte solution, which is used for the generation of gas bubbles to drive fluid flow. It should be noted that a pair of interdigitated Pt electrodes are positioned at the bottom of the pumping chamber (on the electrolytic pump microchip, details given in Section 2.2). To ensure sufficient amount of the electrolyte for the bubbles generation, the pumping chamber is designed to be a through hole in a PDMS substrate and is sealed at the top with a glass slide. Then, the volume of the electrolyte becomes dependent on the thickness of the PDMS substrate, which can be easily adjusted during fabrication. Take the thickness of the PDMS substrate to be 4 mm and an area of 6.1×6.1 mm^2, the maximum volume of the electrolyte in the pumping chamber is 149 μL.

The PCR reservoir and oil reservoir are used for the storage of PCR mixture and silicone oil, respectively, prior to the amplification reaction. Two inlets are located in the PCR reservoir and oil reservoir for fluid injection. The maximum volume of PCR mixture and silicone oil that can be introduced to the CFPCR microchip is 21.3 μL and 14.7 μL, respectively.

The PCR region is divided into four zones: initial denaturation, denaturation, annealing, and extension, as shown in Figure 2.4. In this study, the number of thermal cycles is designed to be 40 for achieving high amplification. The relative duration of the denaturation, annealing, and extension steps are controlled by the microchannel length ratio in the three temperature zones. The ratio used in this work is 1:2:1. The width of microchannel in the PCR region is 100 μm and the height of the microchannel is 125 μm (defined by the photoresist thickness, details given in Section 2.1.2).

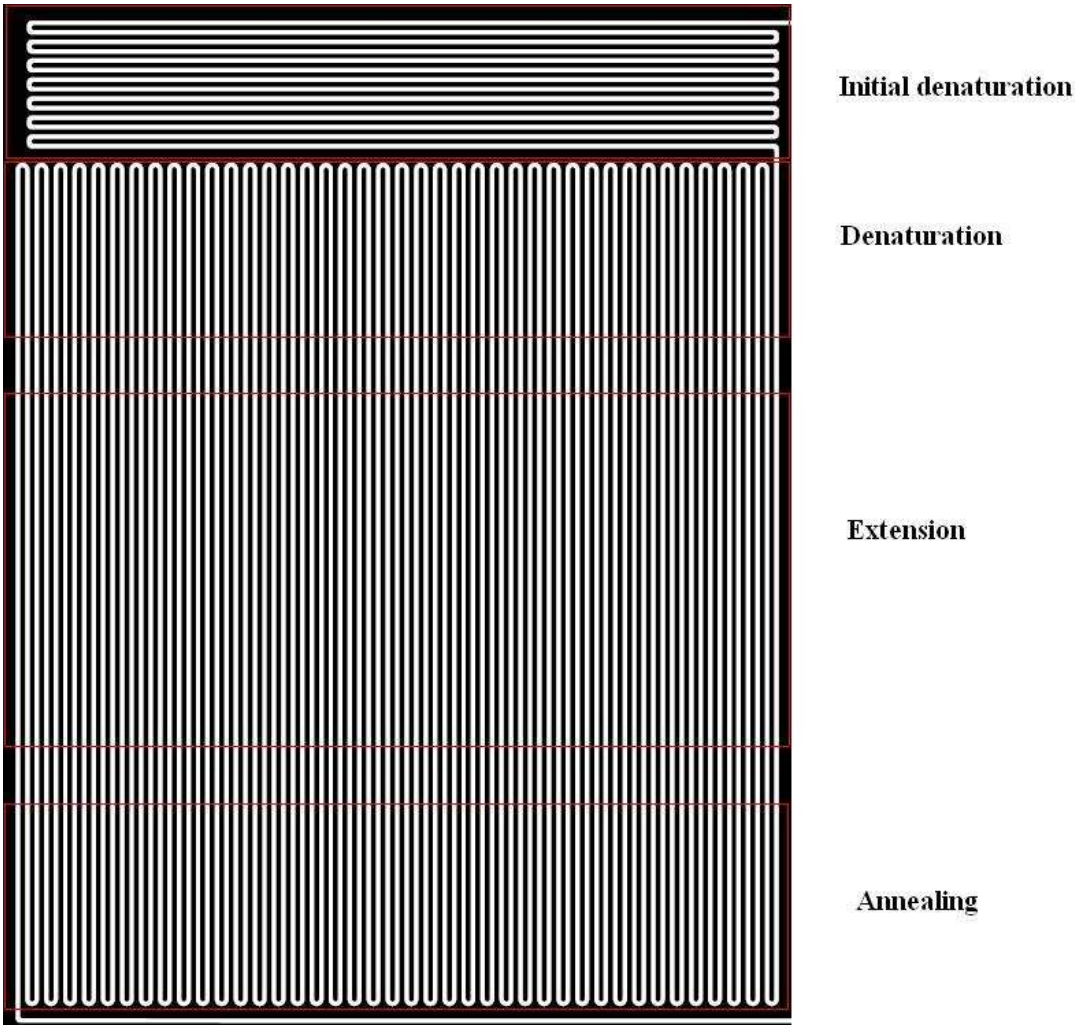

Figure 2.4 PCR region consisting of four zones: initial denaturation, denaturation, annealing, and extension. There are 40 thermal cycles in the CFPCR microchip. The microchannel length ratio in the denaturation, extension, and annealing zones is 1:2:1.

Regarding the fluidic flow, the electrolyte in the pumping chamber is first electrolyzed by the electrolytic pump to form gas bubbles. Pressure is built up inside the pumping chamber, which drives PCR mixture in the PCR reservoir and silicone oil in the oil reservoir through the PCR region to perform DNA amplification.

Finally, the product is collected at the outlet. The fluidic flow within the CFPCR microchip is shown in Figure 2.5.

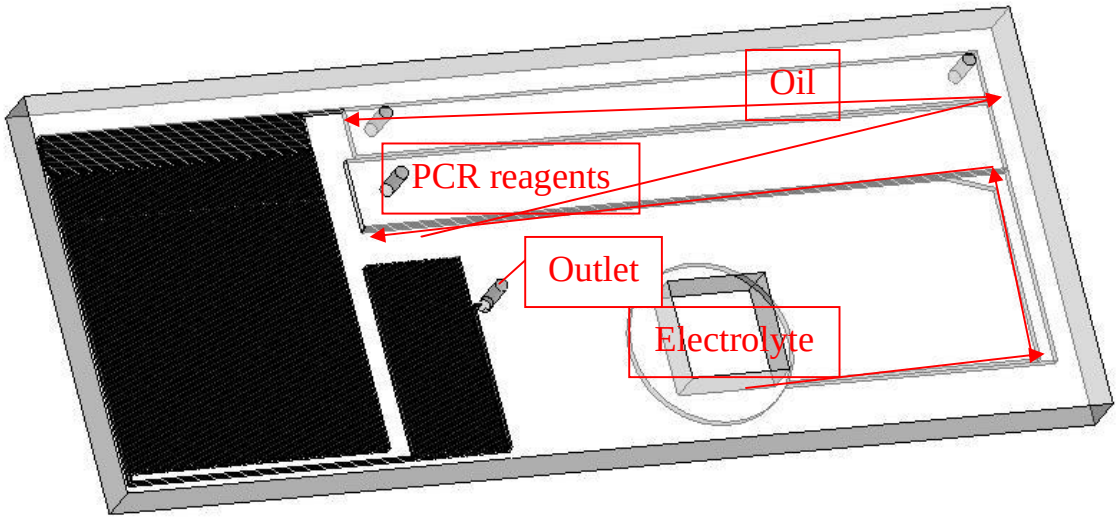

Figure 2.5 Diagram showing the fluidic flow within the microchip.

According to Green *et al.*, the problem of non-specific protein adsorption was related to the geometry of the microchannel. The adsorption problem was reduced for a microchannel with curved turns [120]. Therefore, in this study, microchannel is designed to have curved turns instead of sharp turns, as shown in Figure 2.6.

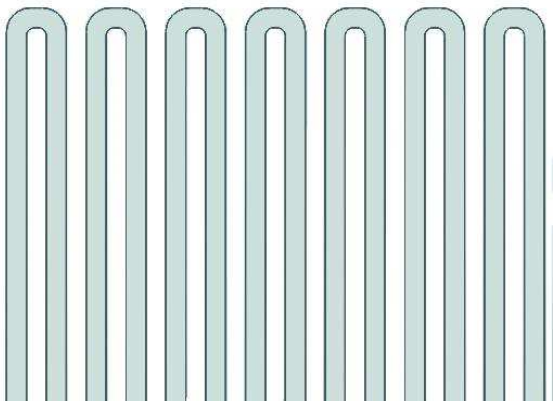

Figure 2.6 Microchannel with curved turns.

2.1.2 Fabrication of CFPCR Microchip

The CFPCR microchip was fabricated using soft lithographic technique using silicon as a substrate, as shown in Figure 2.7. Photolithography was performed to fabricate the CFPCR microchip pattern on the silicon substrate. To achieve high process reliability, the silicon substrate was cleaned and dried prior to the coating of photoresist. The silicon substrate was cleaned with a piranha solution (H_2SO_4:H_2O_2 = 10:1) for 15 min, followed by a deionized water rinse and dehydration on a hot plate (200 °C). A negative photoresist (SU-8 2050) was spun on the silicon wafer at 1,500 rpm to produce a thin uniform layer (125 μm) and was then baked at 95 °C for 15 min. The pattern of the CFPCR microchip was photolithographically transferred to the SU-8 photoresist, followed by baking at 95 °C for 10 min. Then, it was incubated in SU-8 developer for 10 min, washed in isopropyl alcohol, distilled water, and then baked at 200 °C for 2 h. After the fabrication of the silicon master, silicone elastomer and its curing agent (Dow Corning, USA) were mixed in a ratio of 10:1 and poured onto the master. Then, it was degassed under vacuum for 30 min,

cured at 80 °C for 1 h, and peeled from the master. The inlets and outlet were formed by needle-punch and the pumping chamber was formed by cutter-pierce.

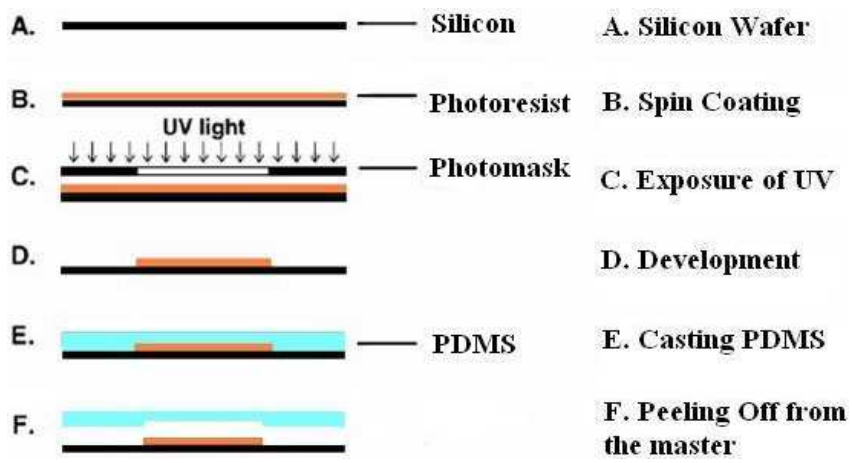

Figure 2.7 Schematic illustrating the CFPCR microchip fabrication procedures using soft lithographic technique.

Figure 2.8 A photograph showing the PDMS CFPCR microchip.

2.2 Electrolytic Pump

In this section, the design of the electrolytic pump is discussed in Section 2.2.1. Then, the fabrication procedures for the electrolytic pump on a glass substrate are detailed in Section 2.2.2. Finally, the control of the electrolytic pump is discussed in Section 2.2.3.

2.2.1 Design of Electrolytic Pump

The main function of the electrolytic pump is to drive all the silicone oil and PCR mixture through the PCR region so that the PCR product can be collected at the outlet of the CFPCR microchip. In view of this, the volume of the gas bubbles generated by the electrolytic pump must be larger than the total volume of the PCR reservoir (21.3 μL), oil reservoir (14.7 μL), and microchannel in the PCR region (27.5 μL, as the total length is 2.2 m), i.e., 63.5 μL.

According to Cameron *et al.*, the theoretical maximum strain resulted from the generated bubbles was about 136,000% under isobaric conditions. Given that the volume of the electrolyte stored in the pumping chamber is 149 μL, the maximum volume of gas bubbles generated is 203 mL, which is much greater than 63.5 μL. Therefore, the volume of the designed electrolytic pumping chamber suffices for driving all the PCR mixture to the outlet.

The electrolytic pump consisted of a pair of interdigitated Pt electrodes, as shown in Figure 2.9. The detailed dimensions are shown in Figure 2.10. This electrode

geometry could improve the pumping efficiency by reducing the current path through the solution as well as lowering the heat generation [77].

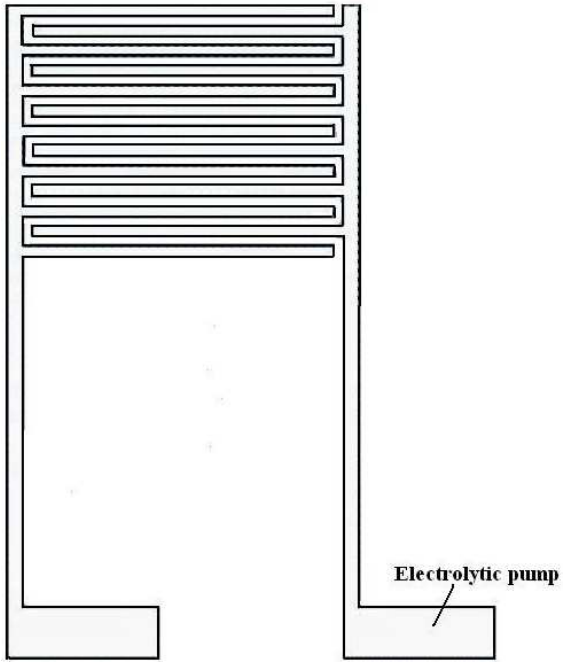

Figure 2.9 A pair of interdigitated Pt electrodes for the electrolysis of water.

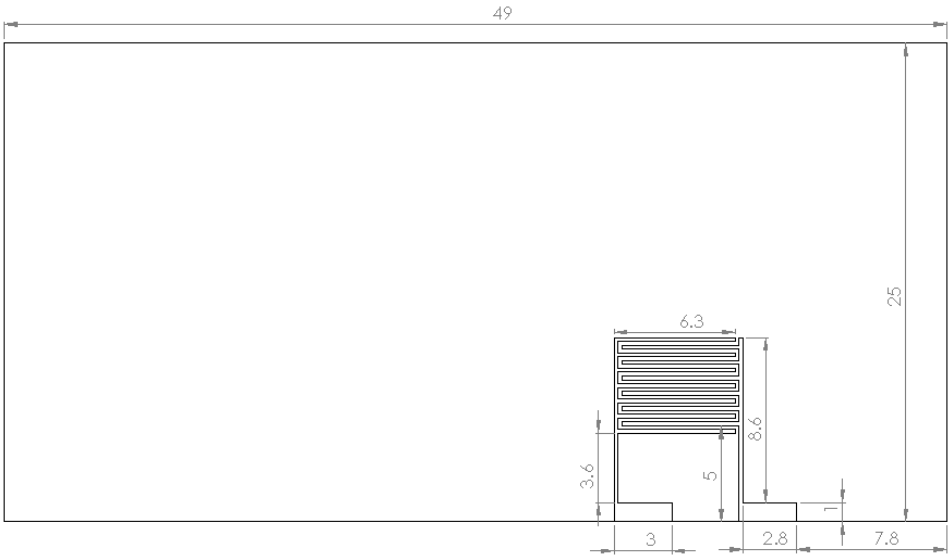

Figure 2.10 Detailed dimensions (expressed in mm) of the electrolytic pump.

2.2.2 Fabrication of Electrolytic Pump

The electrolytic pump was fabricated on a glass substrate using lift-off process, as shown in Figure 2.11. First, the glass substrate was cleaned with a piranha solution (H_2SO_4:H_2O_2 = 10:1) for 10 min, followed by a deionized water rinse and dehydration on a hot plate (200 °C). Then, a positive photoresist (AZ 4620) was spun at 3,500 rpm on the glass substrate to produce a thin uniform layer and was baked at 110 °C for 3 min. The pattern of the electrolytic pump was photolithographically transferred to the photoresist. It was incubated in the AZ developer for 2 min, followed by washing in distilled water. Titanium (Ti, 10 nm) and Pt (100 nm) were sequentially sputtered onto the patterned glass substrate. After that, the AZ photoresist layer (together with the Ti and Pt on top) was removed by acetone in an ultrasonic bath, followed by deionized water rinse.

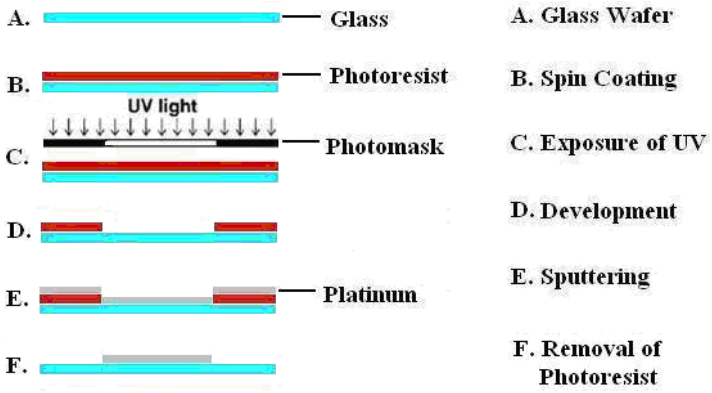

Figure 2.11 Schematic illustrating the electrolytic pump microchip fabrication procedures using lift-off process.

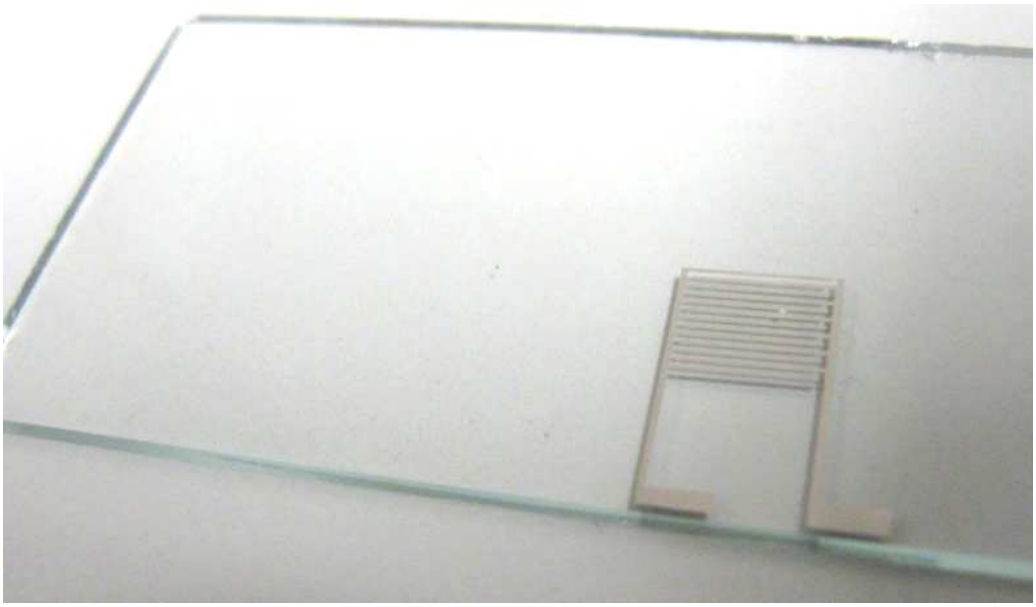

Figure 2.12 A photograph showing the electrolytic pump microchip.

2.2.3 Control of Electrolytic Pump

The electrolytic pump was driven by constant voltage or constant current. For constant voltage, 3 V was applied, unless otherwise specified. For constant current, four different levels were tested (i.e., 350, 400, 440, and 480 μA). A 3-terminal adjustable current source (LM334 from Texas Instruments, USA) was used. The input voltage for LM334 was controlled by LabVIEW (National Instruments, USA), as shown in Figure 2.13. A proportional–integral–derivative (PID) algorithm was used in LabVIEW.

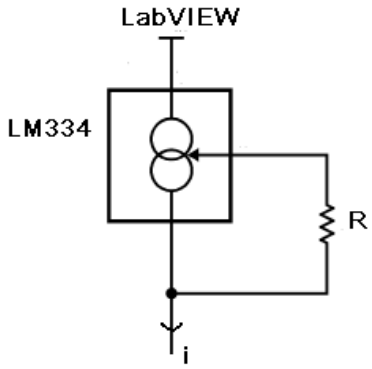

Figure 2.13 Circuit diagram for the constant current circuit.

The PID algorithm adjusts the output of the system to a setpoint by a control loop feedback mechanism. The proportional, integral and derivative terms are summed to determine the output of the PID controller. The algorithm of the PID controller is as follows:

$$V = V_s + K_P * E + K_I * \int_0^t E * dt + K_D * \frac{dE}{dt}$$

Where:

V = Control variable
V_S = Output Set point
K_P = Proportional gain
E = Error
K_I = Integral gain
K_D = Derivative gain
t = Time

The proportional (P), integral (I) and derivative (D) gain, upper limit, lower limit were inputted in the PID to determine the input voltage to LM334. To calculate the error of current between the actual value and the setpoint, the input current of the electrolytic pump was feedbacked to PID to adjust the input voltage to LM334. The PID control programs are shown in Figure 2.14 to Figure 2.19.

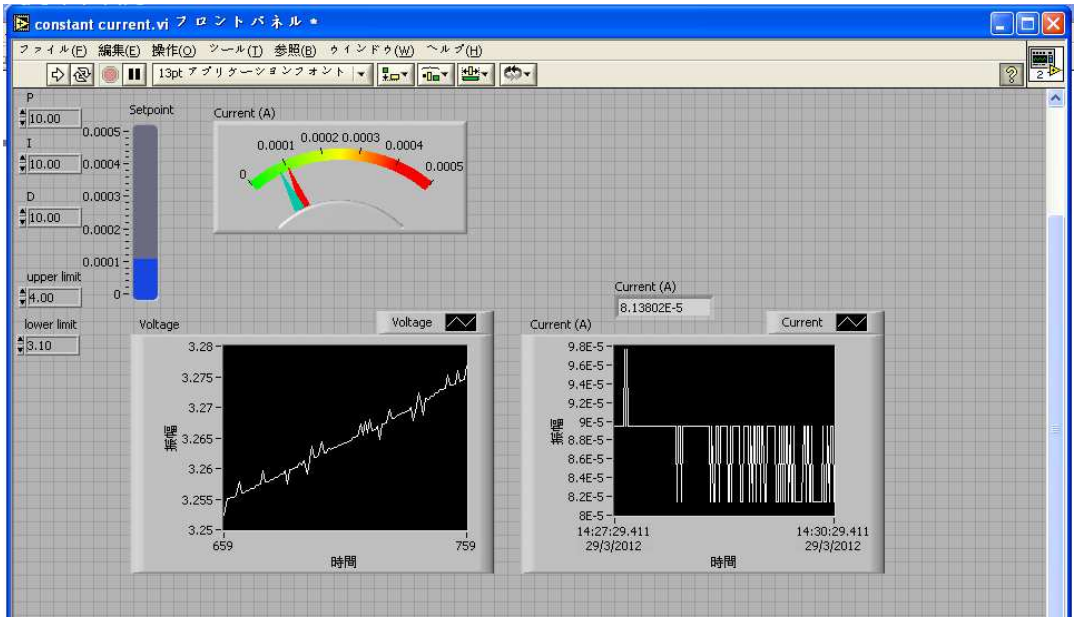

Figure 2.14 Front panel of the LabVIEW program.

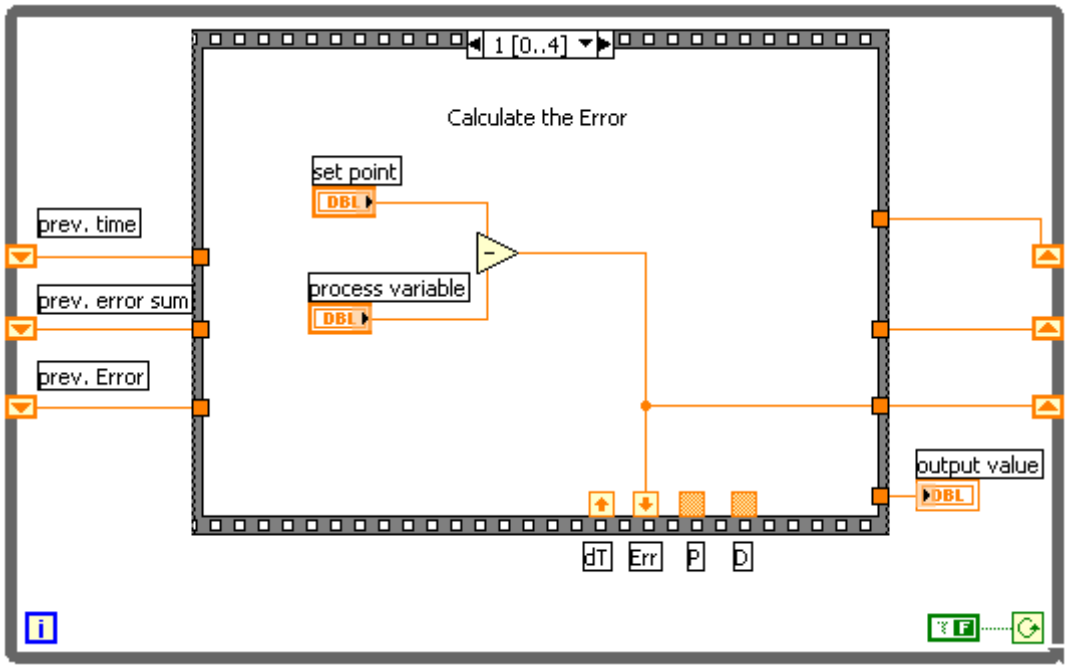

Figure 2.15 Calculation of the error in PID.

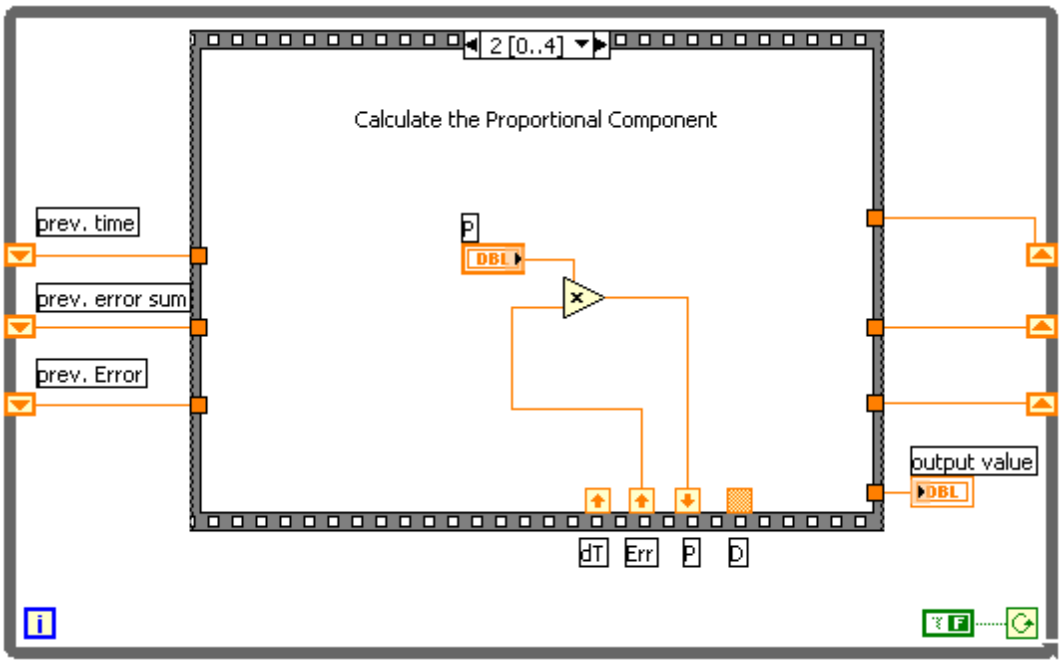

Figure 2.16 Calculation of the proportional component in PID.

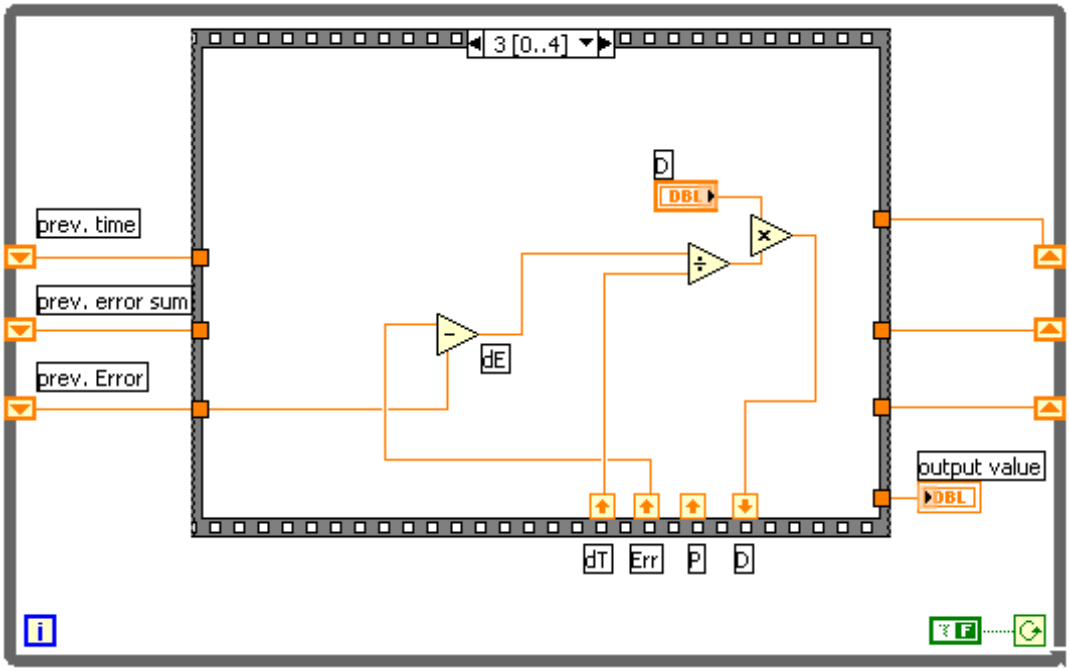

Figure 2.17 Calculation of the derivative component in PID.

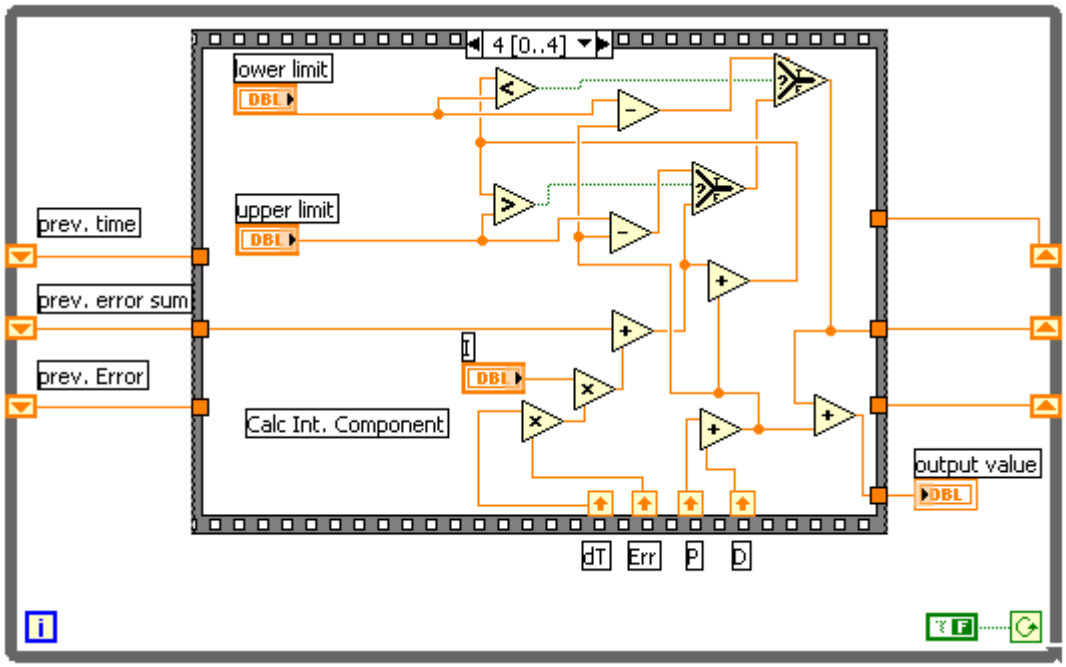

Figure 2.18 Calculation of the integral component and the output value in PID.

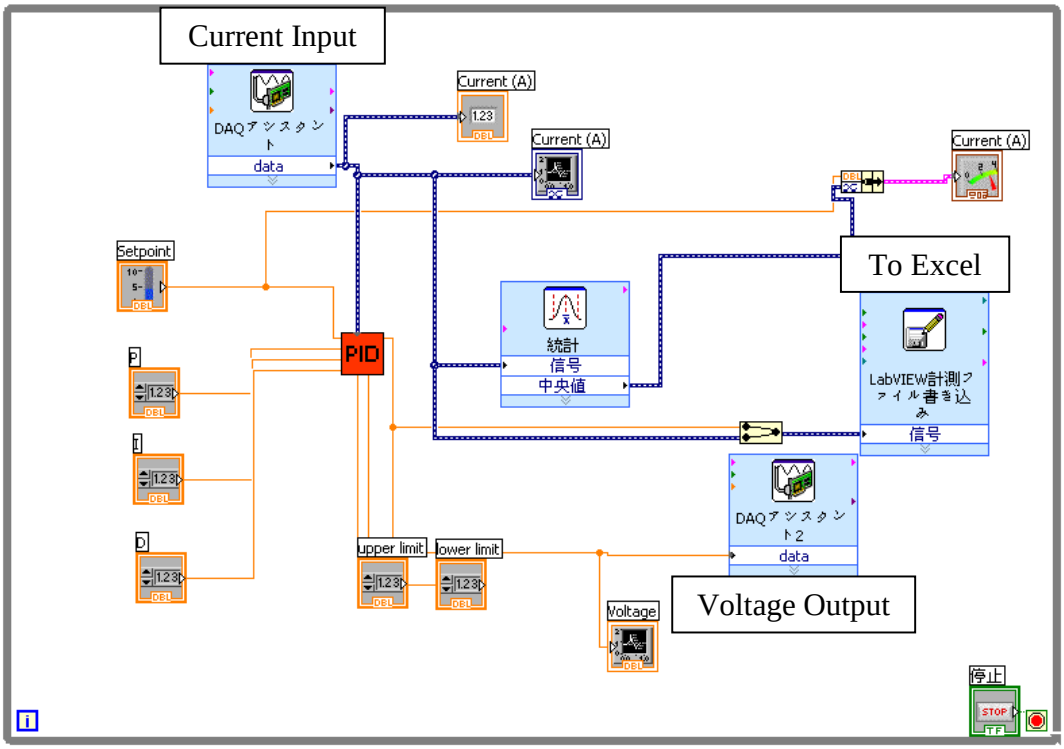

Figure 2.19 Block diagram of the whole PID control. Current Input measured the input current to the electrolytic pump. PID calculated the input voltage to LM334 based on the measured current. Voltage Output measured the applied voltage to LM334. To Excel wrote data (Applied current to the electrolytic pump and applied voltage to the LM334) to an excel file.

2.3 Bonding of CFPCR and Electrolytic Pump Microchips

The CFPCR microchip was bonded to the electrolytic pump microchip by plasma bonding technique. Prior to the plasma treatment, the CFPCR and electrolytic pump microchips were cleaned with acetone, ethanol, and deionized water under sonication for 5 min each, followed by drying in an oven at 80 °C for 1 h. Then, the cleaned microchips were put inside the chamber of plasma cleaner (Harrick, USA). Vacuum pump was used to reduce the pressure of the chamber for plasma generation and the plasma cleaner was turned on to the highest power for 1 min to achieve plasma bonding. Immediately after taken out from the plasma cleaner, the CFPCR and electrolytic pump microchips were aligned, brought into contact, and bonded (Figure 2.20).

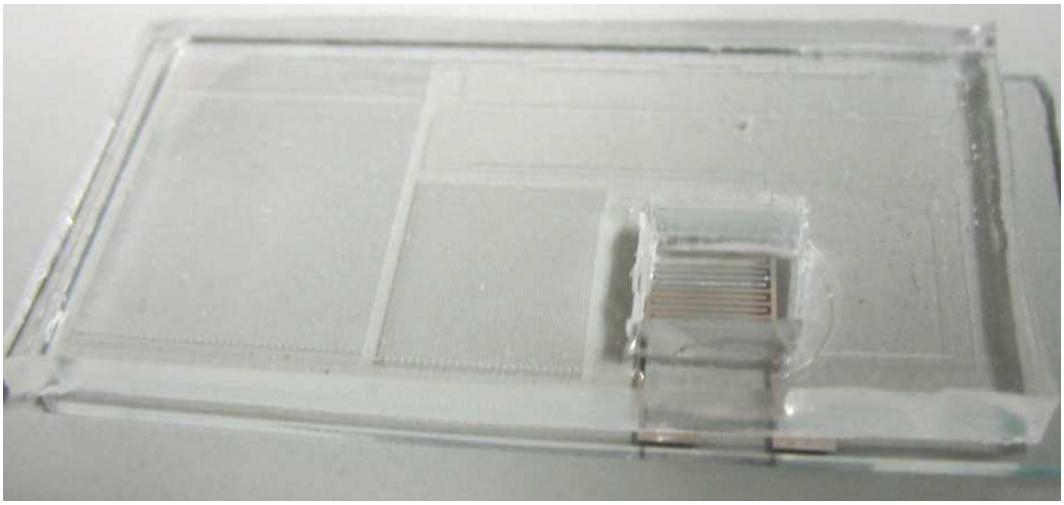

Figure 2.20 A photograph showing the bonded CFPCR and electrolytic pump microchips.

2.4 Temperature Control System

In this section, the design, fabrication, and control of the temperature control system are provided in Section 2.4.1, Section 2.4.2, and Section 2.4.3, respectively.

2.4.1 Design of Temperature Control System

PCR requires very precise temperature control. In this study, the temperature control system comprises metal blocks, thermal sensors, resistors, and other electronic components. The geometry design of the metal blocks is based on the relative duration of the denaturation, annealing, and extension steps of the CFPCR microchip, as shown in Figure 2.21. A feedback control is used for the temperature control system, as shown in Figure 2.22. The potential drawn by the resistance of the thermal sensor is compared with a reference value by using a comparator (LM393 from Texas Instruments). When the potential of the thermal sensor exceeds

the reference value, the output of the comparator would be ground, i.e., no heat would be generated. If the potential of the thermal sensor is below the reference value, voltage is applied to the resistor, which in turn increases the temperature of the metal block. The detailed dimensions of the metal blocks are shown in Figure 2.23.

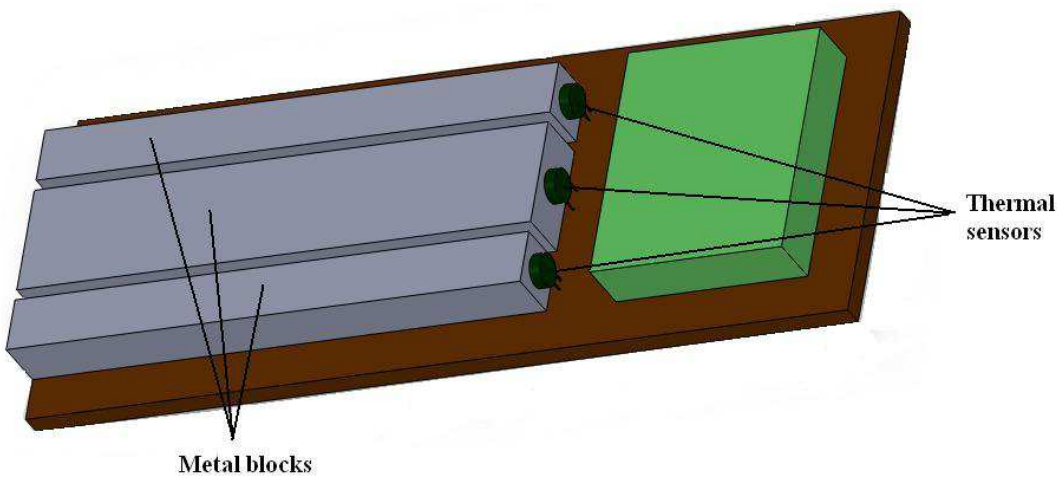

Figure 2.21 Design of the temperature control system.

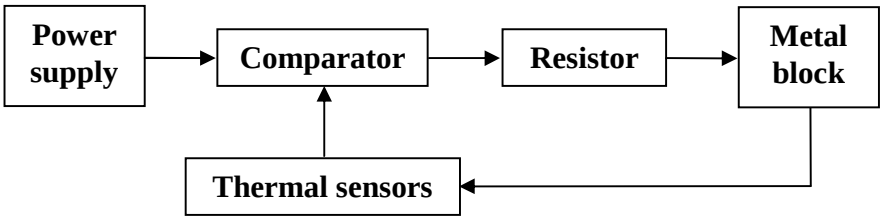

Figure 2.22 A flow chart illustrating the temperature control system for the CFPCR device.

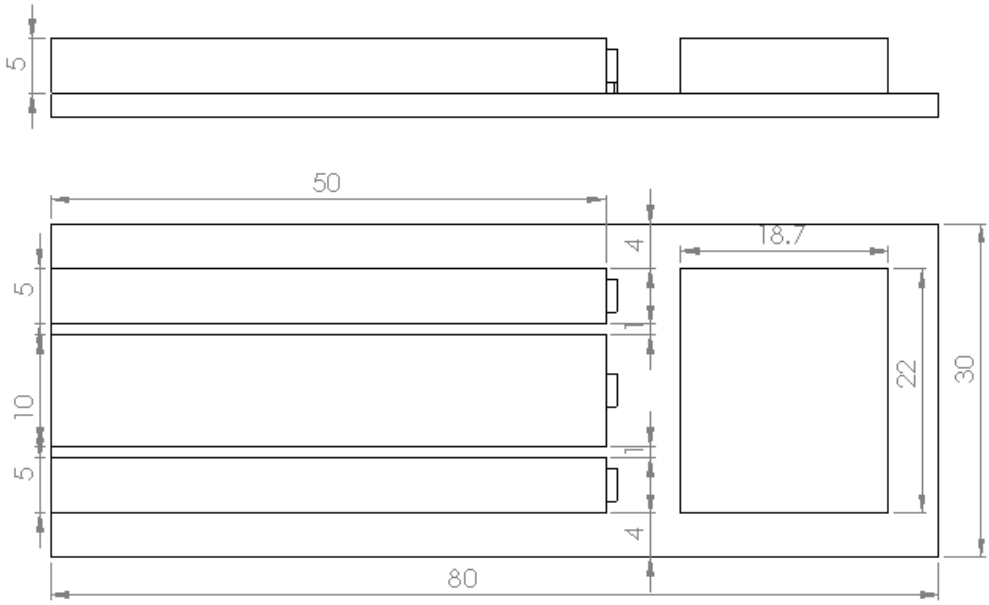

Figure 2.23 Detailed dimensions (expressed in mm) of the heating elements. (top) Cross-sectional and (bottom) top views.

Resistive heating is used for the heating process. By applying a constant voltage, the ideal heating power is given by:

$$P = \frac{V^2}{R} \tag{4}$$

where P is the power, V is the applied voltage, and R is the resistance of the resistor. The temperature can be controlled by adjusting the applied voltage to the resistor.

2.4.2 Fabrication of Temperature Control System

Each heater and thermal sensor set was built according to the circuit diagram as shown in Figure 2.24. A voltage of 9 V was applied to the circuit. R1 was used to adjust the target temperature of the heater by changing the reference voltage of the

LM393. When the applied voltage of the non-inverting input (+) was greater than the inverting input (–) of the LM393, the output of the LM393 was on. As the output was connected to the gate of the RFD14N05, this would turn on the RFD14N05 and the heater. R2 was used to adjust the voltage to each heater for the temperature adjustment. Photographs of the fabricated temperature control system are given in Figure 2.25 and Figure 2.26.

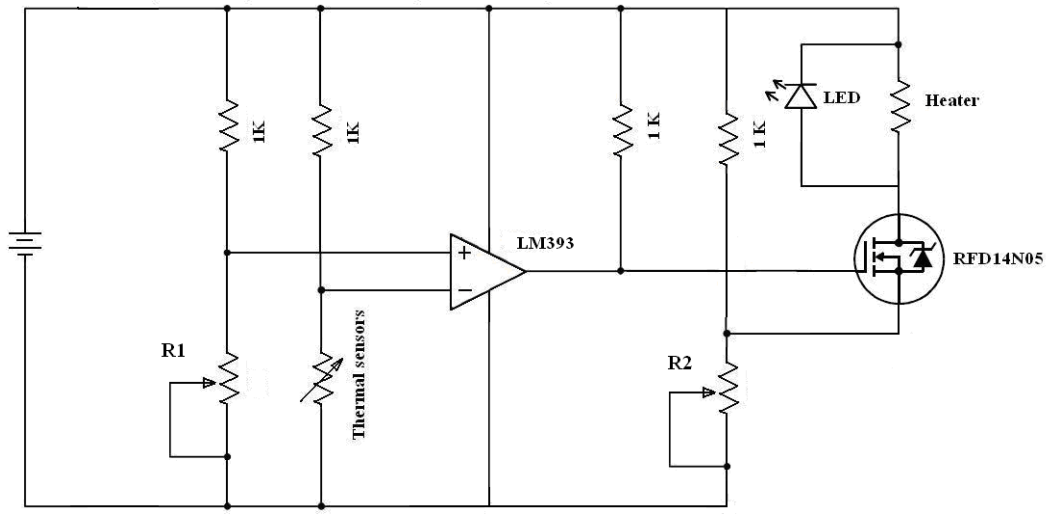

Figure 2.24 Circuit diagram for the temperature control system.

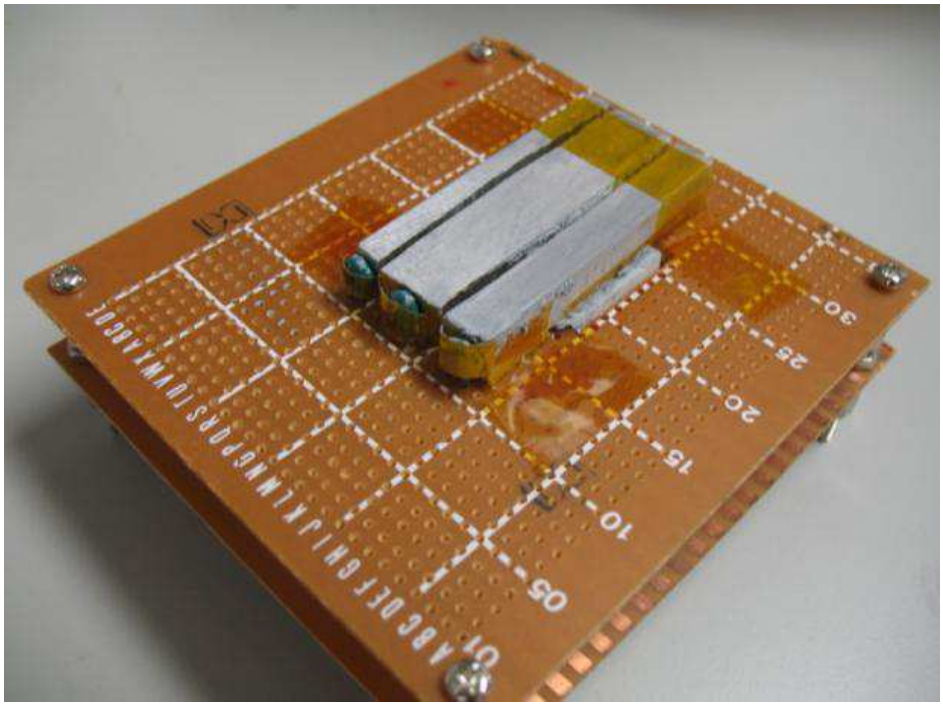

Figure 2.25 A photograph showing the heaters.

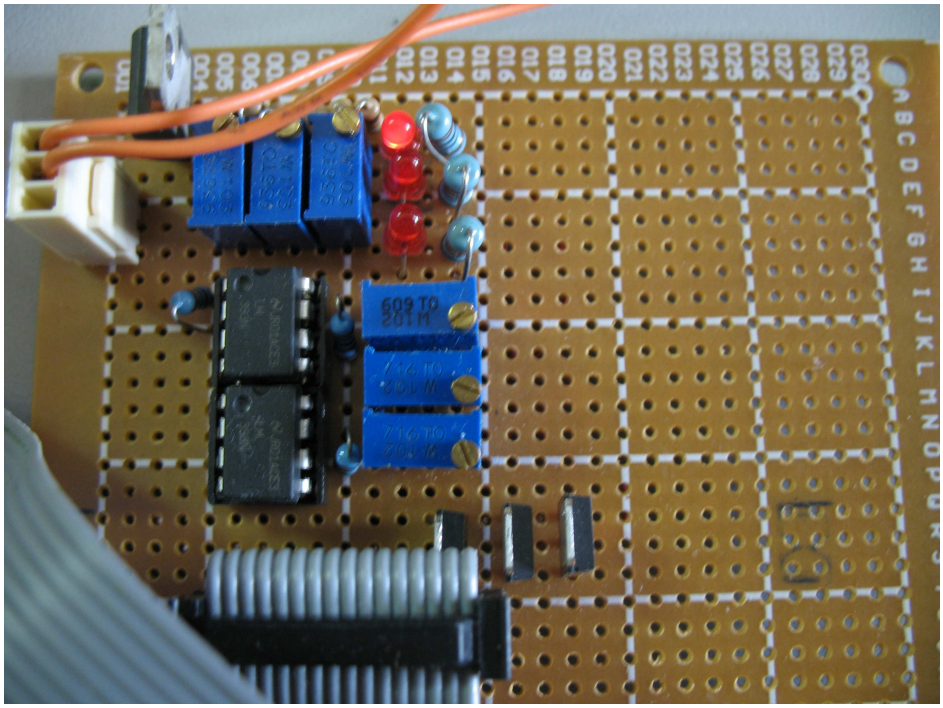

Figure 2.26 A photograph showing the circuit of the temperature control system.

2.4.3 Calibration of Temperature Control System

The temperature control system was calibrated by measuring the surface temperature of a glass substrate (same as the electrolytic pump glass substrate) placed on top of the heater. The power applied to the heater was adjusted by changing the resistance of a variable resistor (R2) until the voltage is high enough to achieve the desired temperature. Then the variable resistor (R1) was adjusted to turn off the heater when the actual temperature is higher than the desired temperature. Take the calibration of heater for 94 °C as an example, the voltage to the heater was increased to about 8 V by increasing the resistance of the variable resistor (R2). When the temperature was higher than 94 °C, the resistance of the variable resistor (R1) was reduced to lower the reference temperature and vice versus.

2.5 PCR Experiments

Apart from thermal cycling profile, PCR amplification efficiency is influenced by many factors such as reaction mixture and surface passivation of the reaction chamber surface. To optimize the amplification efficiency of the CFPCR device, the effects of the presence of a silicone oil plug in front of the PCR mixture (Section 2.5.2.1), concentration of Taq DNA polymerase (Section 2.5.2.2), and surface passivation with BSA (Section 2.5.2.3) are studied. In addition, the effect of amplification time is investigated in Section 2.5.2.4. Finally, the performance of the electrolytic pump is investigated in Section 2.5.2.5.

2.5.1 PCR Protocol

All PCR reagents were purchased from Invitrogen (USA), unless otherwise stated. A master mix (20 μL) was prepared for the CFPCR experiments, which contained 4 μL of 5× Green GoTaq® Flexi Buffer (Promega, USA); 1.2 μL of 25 mM $MgCl_2$; 0.4 μL of 10 mM dNTPs (10 mM each of dATP, dCTP, dGTP, and dTTP); 1 μL of 10 μM forward primer (5'-TGGCATTGACCCTGAGTGATT-3'); 1 μL of 10 μM reverse primer (5'-TAATGATACCGATGAAACGAGAGA-3'); 0.5 μL of 5 U/μL Taq DNA polymerase;; 0.2 μL of 1 ng/μL template DNA (pBR322, amplification region: 1732 to 1876); 0, 0.5, or 2 μg/μL of BSA; and UltraPure™ DNase/RNase-free distilled water.

2.5.2 Experimental Setup

Prior to using the electrolytic pump for the CFPCR device, a syringe pump was used in studying the effects of silicone oil, concentration of Taq DNA polymerase, surface passivation, and duration of CFPCR on amplification efficiency. A syringe needle was glued to the pumping chamber of the CFPCR microchip by using epoxy (Alteco, Japan), as shown in Figure 2.27. To perform CFPCR, PCR reagent and silicone oil (Invitrogen) were injected to the PCR reservoir and oil reservoir through two inlets, respectively. Then, all inlets were sealed with a polyimide film tape (3M, USA). A glass slide was bonded on top of the film tape using double-sided adhesive tape. After that, the CFPCR microchip was aligned onto the temperature control system and the syringe pump was used to create the desired flow rate. Finally, the products were collected at the outlet with a pipette tip.

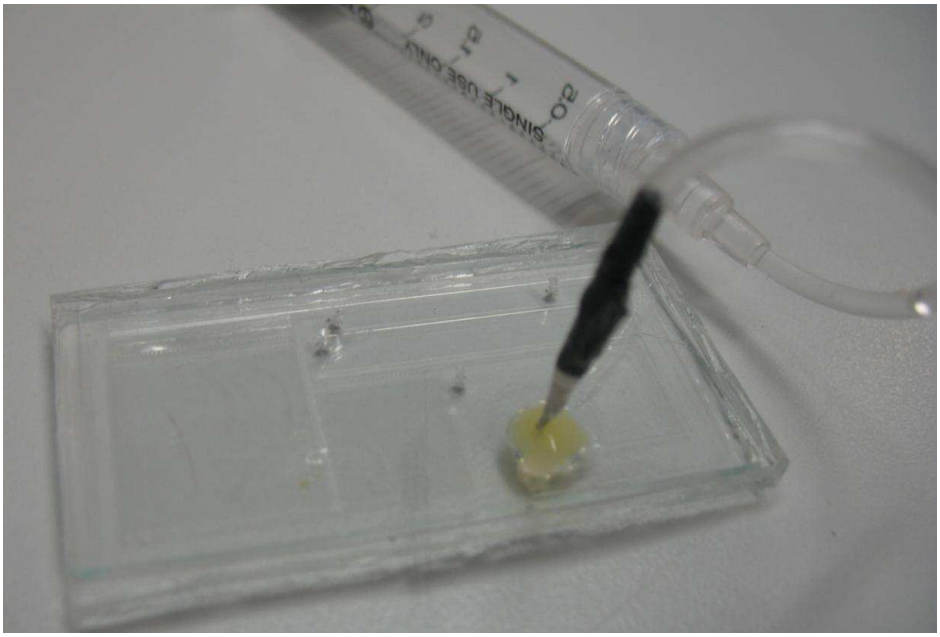

Figure 2.27 A photograph showing the CFPCR microchip with syringe.

Figure 2.28 A photograph showing the syringe pump.

2.5.2.1 Effect of Silicone Oil

The fluidic flow is an important issue in CFPCR. According to Nakayama *et al.*, the introduction of an oil plug in front of the PCR reagent could ensure the stability of the flow. To test this in our CFPCR device, 10 μL of silicone oil (Invitrogen, USA) was introduced to the oil reservoir. A control experiment was performed without the oil plug.

2.5.2.2 Effect of Concentration of Taq DNA Polymerase

Taq DNA polymerase was likely to be adsorbed to the surface of the PDMS microchip [4] . Therefore, the amount of Taq DNA polymerase in the PCR reagent was critical to the amplification efficiency. The effect of different concentrations of Taq DNA polymerase was studied by changing the concentration of Taq DNA polymerase in the PCR reagent. In this study, 0.5, 1.5, and 2.5 units/20 μL of Taq DNA polymerase were tested.

2.5.2.3 Effect of Surface Passivation

To avoid the non-specific adsorption of PCR reagent to the wall of the microchip, BSA was used as a surface passivation agent. Both dynamic and static passivations were studied. To study the effect of dynamic passivation, PCR reagents with 0, 0.5, and 2 μg/μL BSA (Biolabs, UK) were prepared to perform CFPCR. To study the effect of static passivation, the microchannel and reservoir were pretreated with 0, 2, or 5 μg/μL of BSA for 1 h, and followed by drying in oven at 80 °C for 1 h.

2.5.2.4 Effect of CFPCR Duration

The fast thermal cycling of CFPCR is attractive, but the amplification efficiency may be affected if the cycling time is too short. In this study, the effect of the duration of CFPCR on the amplification efficiency was investigated. The duration of CFPCR was the time for the PCR reagent to pass through the PCR reaction region. It was controlled by changing the flow rate of the syringe pump.

2.5.2.5 Performance of Electrolytic Pump

In this study, sodium sulfate (Na_2SO_4) was chosen as the electrolyte solution for the electrolytic pump. The procedures to perform CFPCR by using electrolytic pump were similar to that using syringe pump, except that 200 μL of 1 M Na_2SO_4 was added to the pumping chamber for the former one. The pumping chamber was then sealed with a polyimide film tape, followed by the bonding of a glass slide on it using double-sided adhesive tape. Finally, the CFPCR microchip was aligned onto the temperature control system and constant voltage/current was applied to the electrolytic pump for the generation of the gas bubbles.

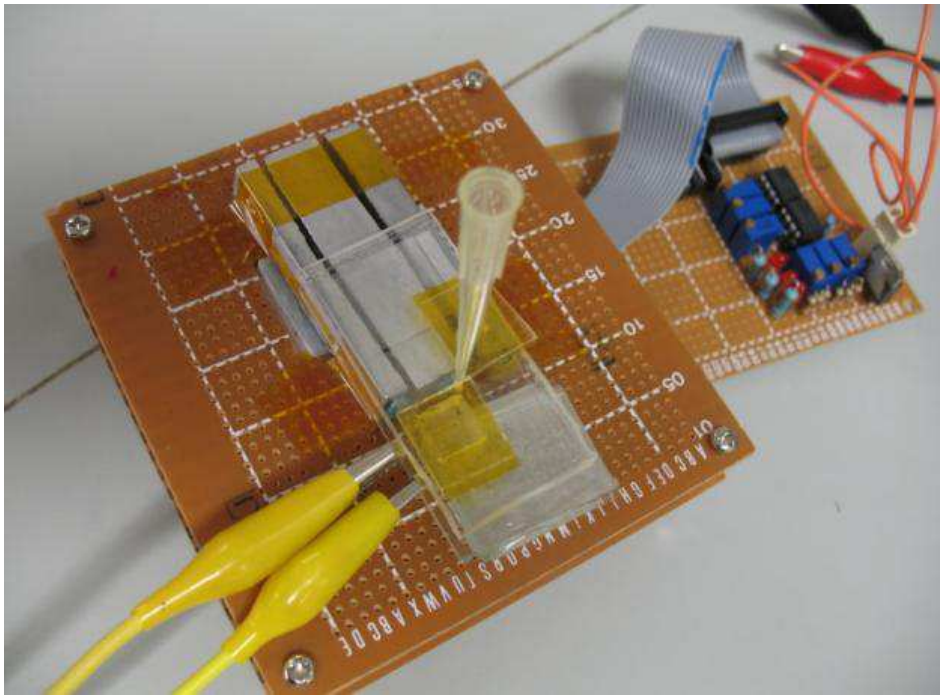

Figure 2.29 A photograph showing the setup of the CFPCR device with electrolytic pump.

2.5.3 Agarose Gel Electrophoresis

A 3% agarose gel was prepared by dissolving 0.9 g of UltraPure™ Agarose (Invitrogen) in 30 mL of 0.5× Tris-borate-EDTA (TBE) buffer. Then, it was heated in a microwave oven, followed by cooling at room temperature for 1 h. PCR product (10 μL) was loaded into the well of the agarose gel. Electrophoresis was carried out with a voltage of 100 V for 40 min. After that, the gel was immersed in 0.5 μg/mL ethidium bromide for 15 min. Finally, the gel was visualized by UV transillumination.

CHAPTER 3

RESULTS

3.1 Fluidic Flow

3.1.1 Gas Bubbles Generation

One of the essential components of this work is the on-chip generation of gas bubbles by electrolysis so as to drive reaction mixture through the CFPCR microchannel. A fine control of the gas bubbles formation is important to achieve the desired flow rate of CFPCR. Figure 3.1 shows that tiny gas bubbles were generated gradually by applying 3 V to the interdigitated Pt electrodes with an electrolyte solution of 1 M Na_2SO_4. The accumulation of gas bubbles on the electrodes was observed.

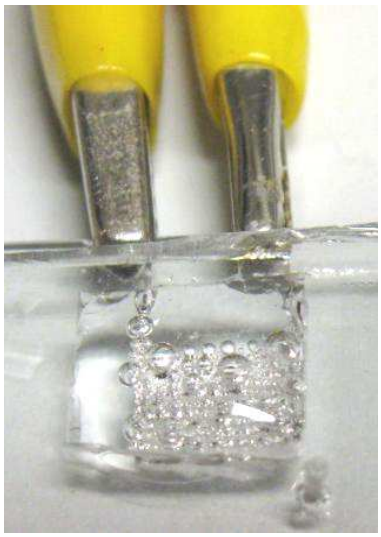

Figure 3.1 A photograph showing the gas bubbles generated by the electrolytic pump.

3.1.2 Control of the Electrolytic Pump using Voltage Source

To compare the performance of syringe pump and electrolytic pump, the characteristics were studied in both pumping mechanisms. The average duration of cycle was calculated and plotted against the speed of syringe pump, as shown in Figure 3.2.

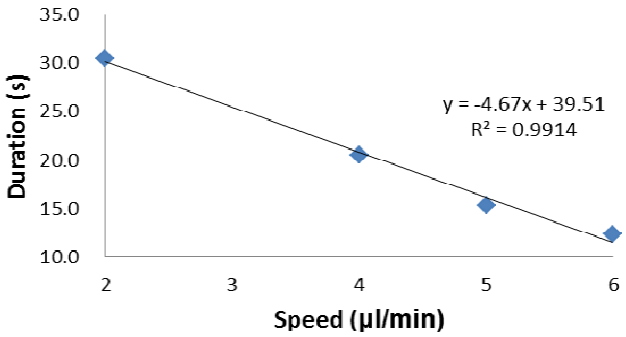

Figure 3.2 Plot of average duration of cycle against the speed of syring pump.

The relationship between CFPCR duration and voltage applied to the electrolytic pump is shown in Figure 3.3. The CFPCR duration decreases with increasing applied voltage as more gas bubbles are produced with higher voltage. It took 22 min to complete CFPCR with an applied voltage of 3 V and 34 min with an applied voltage of 2.8 V.

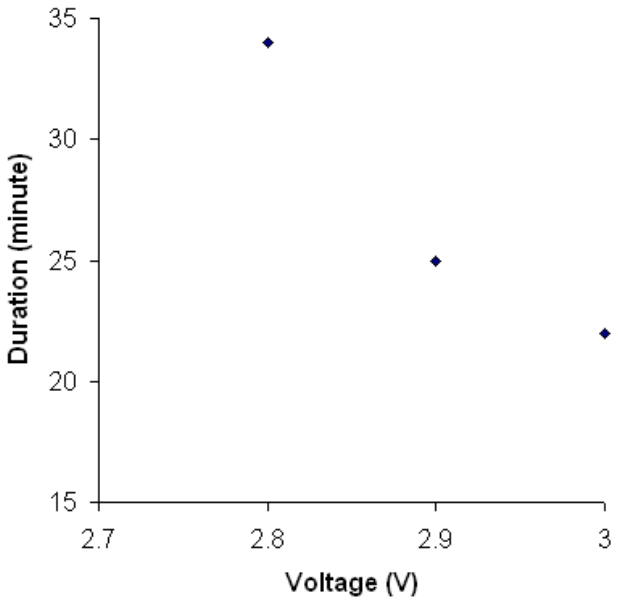

Figure 3.3 Plot of duration of CFPCR against voltage applied to the electrolytic pump.

One important experimental observation with electrolytic pump with voltage control was that the duration in each cycle increased gradully (more than 60% difference between 1st and 20th cycle), as shown in Figure 3.4. Figure 3.5 shows the current of the electrolytic pump dropped gradually when a constant voltage (3 V) was applied. It should be noted that the rate of gas bubbles generation is proportional to the current level.

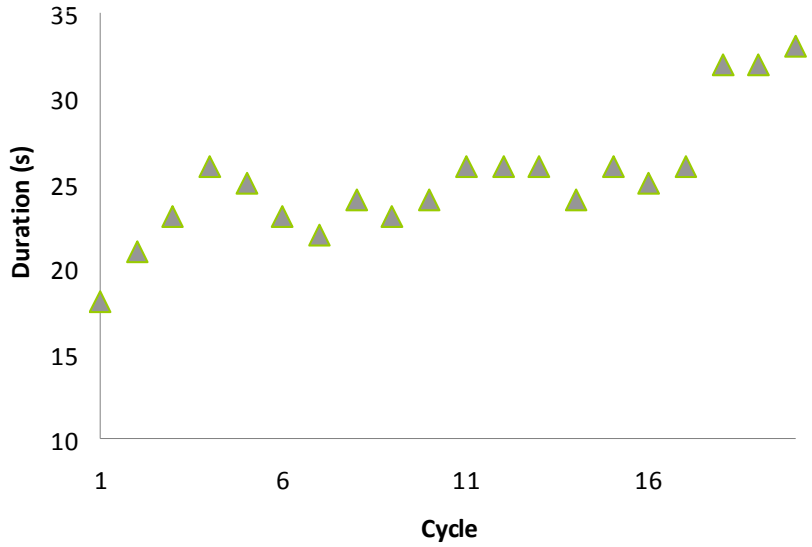

Figure 3.4 Plot of duration in each cycle using electrolytic pump with constant voltage.

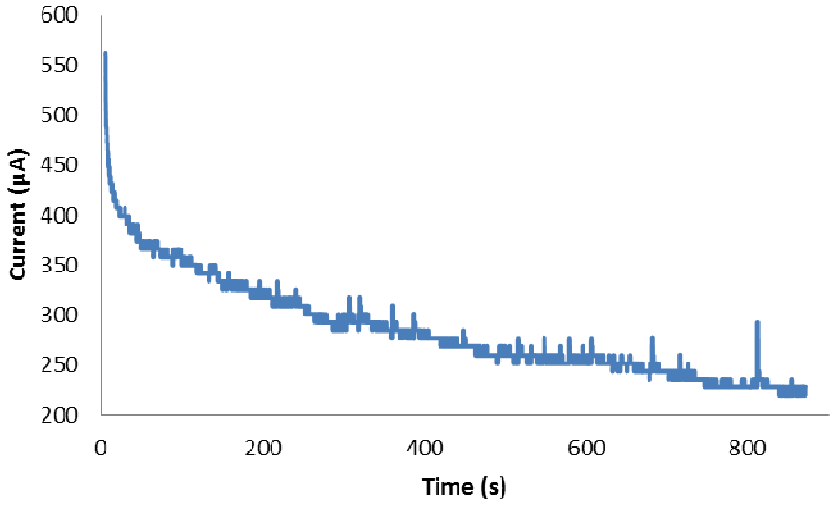

Figure 3.5 Plot of current against time when a constant voltage (3 V) was applied to the electrolytic pump.

3.1.3 Control of the Electrolytic Pump using Current Source

When constant current was applied to the electrolytic pump, the duration in each cycle was more stable than that using constant voltage. The deviation of the maximum and minimum duration to the average duration was less than 20%, as shown in Figure 3.6. When the generated gas bubbles covered the electrode, the voltage was increased to maintain the constant current. Therefore, the gas bubbles generation rate was kept more stable. The relationship between average cycle duration and applied current was shown in Figure 3.7.

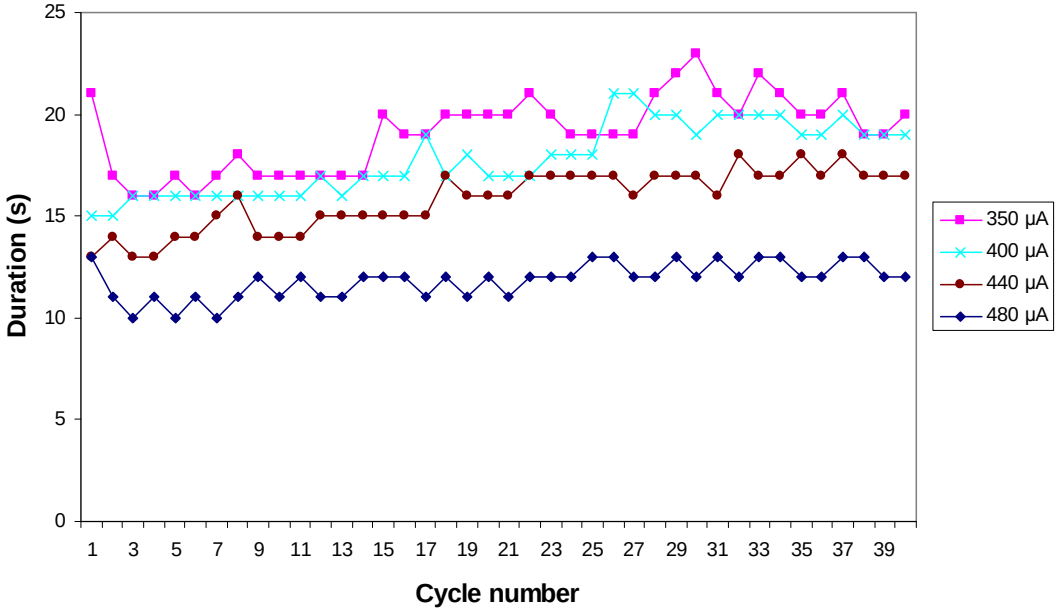

Figure 3.6 Plot of duration in each cycle using electrolytic pump with different currents.

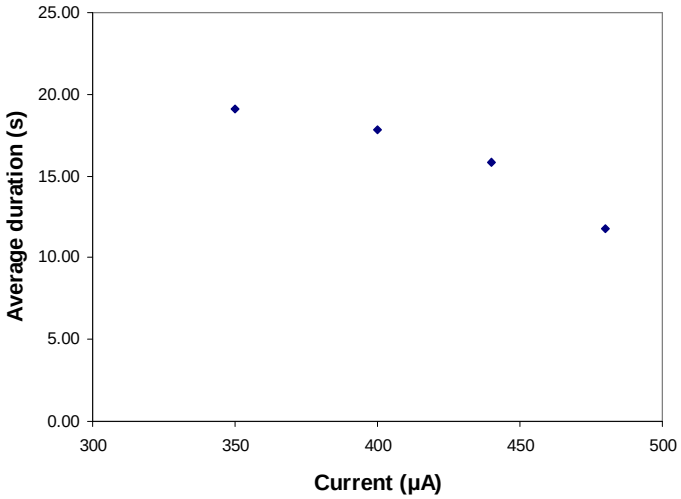

Figure 3.7 Plot of average duration of each cycle against current applied to the electrolytic pump.

3.1.4 Fluidic Flow in CFPCR

Leakage and blockage problems were observed during the CFPCR. The leakage of PCR reagents was observed. This mainly happened in the area near the pumping chamber, as shown in Figure 3.8.

Figure 3.8 A photograph showing the leakage of PCR reagents during the CFPCR. The green PCR reagents leaked out through the space between the glass and PDMS.

PCR involves a high temperature step of denaturation. Typical temperature of the denaturation is 94 °C, which is close to the boiling point of water. At this high

temperature, the evaporation of liquid and the decrease of gas solubility resulted in air gaps formation in the CFPCR microchannel, as shown in Figure 3.9. The fluidic flow was slowed down and eventually stopped by the presence of the air gaps.

Figure 3.9 A photograph of the air gaps formed in the CFPCR microchannel.

The presence of air in the PCR reservoir, oil reservoir, and CFPCR microchannel is detrimental to the flow control. It makes the fluidic flow unstable and even terminates the flow in some cases. In this study, air was easily introduced during the sealing process of the inlets with polyimide film tape, as shown in Figure 3.10. This is because PDMS (the material used for the CFPCR microchip) deforms easily upon force application. Such deformation would compress the fluid inside the reservoir and air would get in when the force is released.

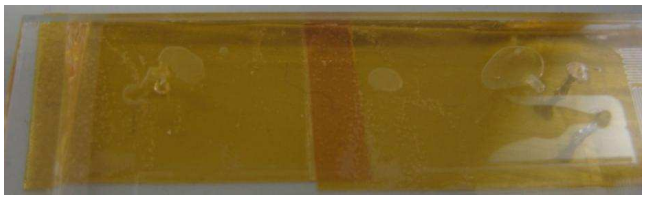

Figure 3.10 A photograph showing air trapped within the reservoir after sealing the inlets with polyimide film tape.

3.2 Temperature Control

Another essential component of CFPCR is temperature control. The calibration curves for the three heaters/metal blocks are shown in Figure 3.11. The plots indicate a linear relationship between temperature of the metal block and square of the voltage. The temperature ramping of the three heaters are shown in Figure 3.12. The three heaters reached the desired temperatures within 25 min.

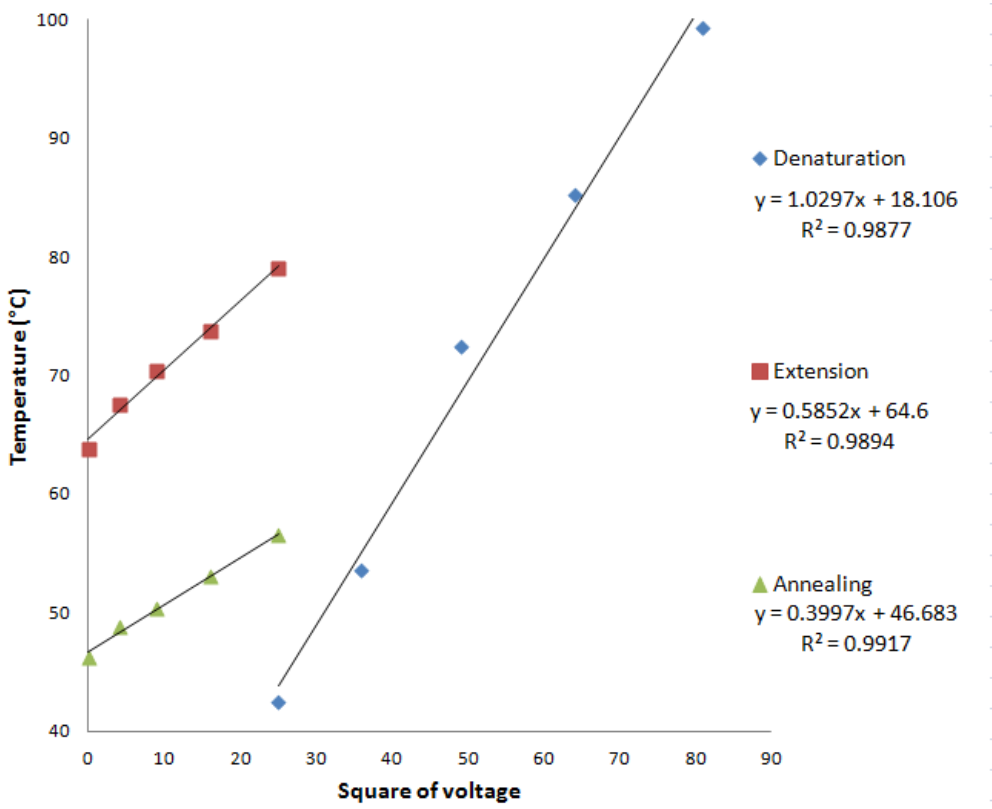

Figure 3.11 Plots of temperature against square of voltage of the three heaters/metal blocks.

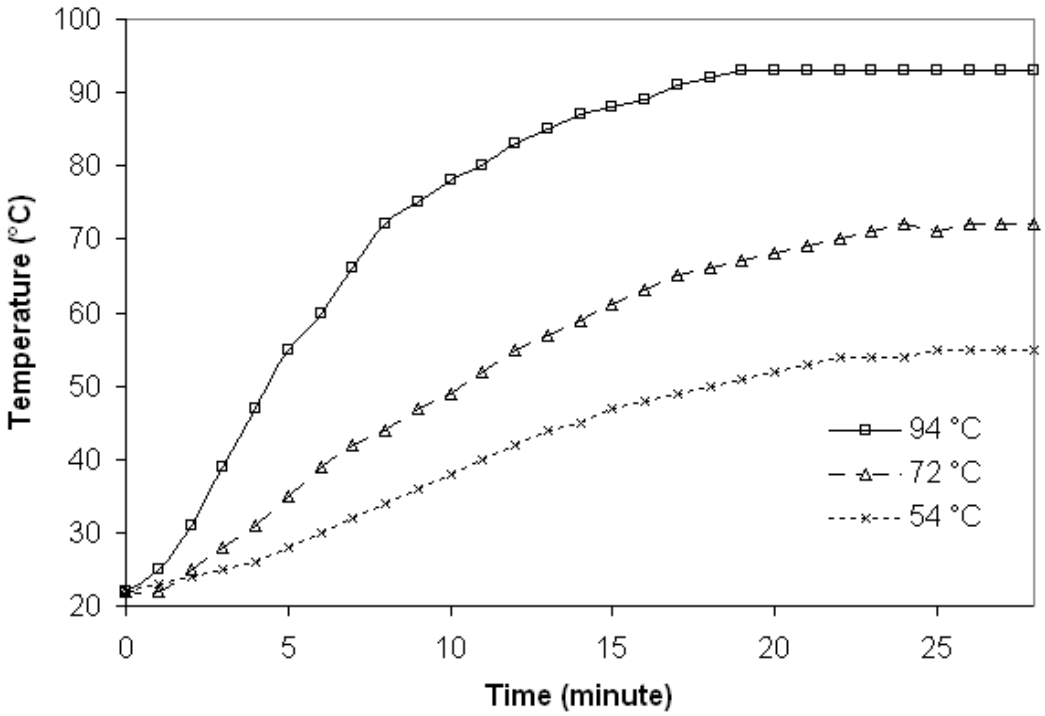

Figure 3.12 Plots of temperature of the three metal blocks against time. The time required for the metal blocks to reach the denaturation, annealing, and extension temperatures were 20, 25, and 25 min, respectively.

3.3 PCR Experiment

3.3.2 Effect of Silicone Oil

In this study, silicone oil was introduced in front of the PCR reagent to eliminate the gas bubbles generation in the microchannel. However, the adsorption of silicone oil by PDMS was observed. Once all silicone oil was adsorbed, the flow of the PCR reagent became unstable, irregular and eventually stopped. Therefore, it is necessary to ensure a sufficient amount of silicone oil in front of the PCR reagent throughout

the entire CFPCR process. The minimum volume of silicone oil needed in our CFPCR microchip was found to be around 8 μL.

3.3.2 Effect of Concentration of Taq DNA Polymerase

The effect of concentration of Taq DNA polymerase on amplification efficiency is shown in Figure 3.13. Three different concentrations (0.5, 1.5, and 2.5 units/20 μL) of Taq DNA polymerase were tested. Weak PCR product bands were observed for 0.5 and 1.5 units/20 μL while a much stronger PCR product band was observed for 2.5 units/20 μL.

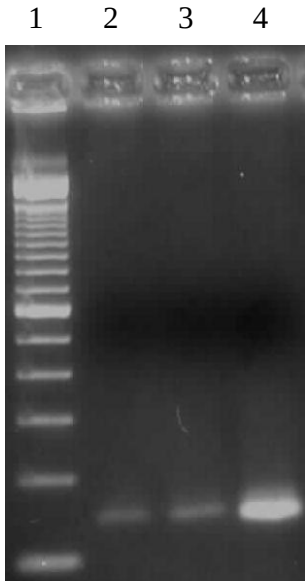

Figure 3.13 Gel electrophoresis image of the amplification results of CFPCR with different concentrations of Taq DNA polymerase. Lane 1 is DNA size marker; lanes 2, 3, and 4 are CFPCR with 0.5, 1.5, and 2.5 units/20 μL Taq DNA polymerase.

3.3.3 Effect of Surface Passivation

Figure 3.14 shows the effect of dynamic coating with different concentrations of BSA. Without BSA, the intensity of the PCR product band was weak. When CFPCR was performed with dynamic passivation using BSA, the intensity of the PCR product band was much brighter than that without BSA. The PCR product band intensity for 2 μg/μL BSA was similar to that for 0.5 μg/μL BSA.

Figure 3.14 Gel electrophoresis image of the amplification results of CFPCR with dynamic passivation using different concentrations of BSA. Lane 1 is DNA size marker; lanes 2, 3, and 4 are CFPCR with 2, 0.5, and 0 μg/μL BSA.

Figure 3.15 shows the effect of static coating with different concentrations of BSA. As expected, the intensity of the PCR product band with BSA was stronger than that without BSA. Besides, it was noted that the intensity of the PCR product band for 5 μg/μL BSA was weaker than that for 2 μg/μL BSA. The unstable flow of the reagents was observed for 5 μg/μL BSA.

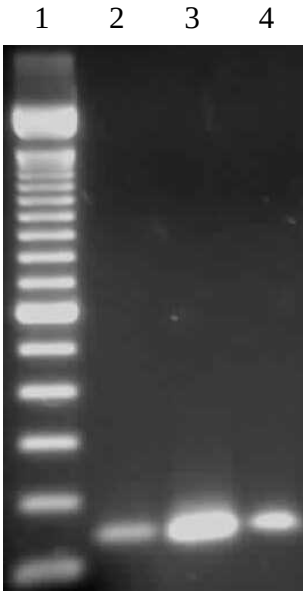

Figure 3.15 Gel electrophoresis image of the amplification results of CFPCR with static passivation. Lane 1 is DNA size marker; lanes 2, 3, and 4 are CFPCR with 0, 2, and 5 μg/μL BSA, respectively.

3.3.4 Effect of CFPCR Duration

The effect of the duration of CFPCR is shown in Figure 3.16. With CFPCR duration of 20 min, an observable PCR product band was obtained. This amplification time is much shorter than that of the conventional PCR thermal cycler (about 1–2 h). In fact, the intensity of the PCR product band for the 20-min CFPCR was weaker than that of 32-min CFPCR.

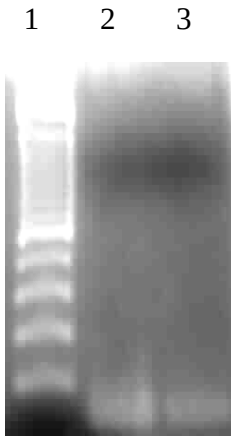

Figure 3.16 Gel electrophoresis image of the amplification results of CFPCR with different durations using syringe pump. Lane 1 is DNA size marker; lanes 2 and 3 are CFPCR of 32 and 20 min, respectively.

3.3.5 Performance of Electrolytic Pump

After the above optimization with syringe pump, CFPCR was performed using the electrolytic pump to drive the PCR reagent through the microchannel. As shown in Figure 3.17, the target sequence was successfully amplified. The amplification time for the electrolytic pump-driven CFPCR was 22 min. This result illustrates that our CFPCR device with the on-chip electrolytic pump could achieve DNA amplification in point-of-care or on-site setting.

Figure 3.17 Gel electrophoresis image of the amplification results of CFPCR using electrolytic pump. Lane 1 is DNA size marker; lane 2 is CFPCR using electrolytic pump.

CHAPTER 4

Discussion

4.1 Fluidic Flow

4.1.1 Gas Bubbles Generation

The gas bubbles were generated gradually by applying voltage to the electrodes. The pressure inside the pumping chamber would be increased and used as the pumping force for the movement of the PCR reagent. To perform CFPCR, the fine control of the gas bubbles formation would be critical. In this study, the voltage and current source were used. The performance of different power source would be discussed.

4.1.2 Control of the Electrolytic Pump using Voltage Source

In this study, the average duration of cycle was found to be directly proportional to the injection speed of the commercial syringe pump. To achieve the similar performance by using electrolytic pump, constant voltage and constant current were applied to the electrolytic pump.

The voltage source was studied as it could be controlled easily. The constant voltage was easily achieved by the power supply or battery. It was observed that the duration in each cycle increased gradually (more than 60% difference between 1^{st} and 20^{th} cycle). The main reason was the accumulation of gas bubbles on the electrode surface. The gas bubbles covered the electrode and reduced the effective

electrode surface area for the electrolysis of water. The duration in each cycle would increase gradually as gas bubbles generation decrease gradually. Besides, the decrease in rate of the electrolysis of water was confirmed by the current drop in Figure 3.4. Therefore, the constant voltage was not suitable for CFPCR as the extended duration would affect the efficiency of PCR in each cycle.

4.1.3 Control of the Electrolytic Pump using Current Source

The current source was kept constant by varying the applied voltage to the electrode. When the generated gas bubbles covered the electrode, the current would be decreased. Then, the voltage was increased to maintain the constant current. Therefore, the rate of the electrolysis of water was kept more stable. The results showed that the deviation of the maximum and minimum duration to the average duration was less than 20%. This indicated that constant current source was a better choice than using constant voltage source as the rate of the gas bubbles generation is more stable.

4.1.4 Fluidic Flow in CFPCR

The leakage of the PCR reagent was observed during the CFPCR. As the viscous silicone oil was introduced in front of the PCR reagent, the movement of the PCR reagent was slowed down. If the internal pressure of the PCR reagent builds up to a level that exceeds the bond strength of the PDMS and glass substrates, the leakage of the PCR reagent occurred. To prevent the leakage, the applied flow rate should not increase abruptly. In other words, a gradual increase in the applied pressure

facilitated the silicone oil to move forward smoothly, thereby reducing the internal pressure build-up.

During the denaturation of PCR, the evaporation of liquid and the decrease of gas solubility occurred. The air gaps were formed in the microchannel. Eventually, the fluidic flow was slowed down and stopped. To avoid the termination of the fluidic flow, silicone oil was introduced in front of the PCR reagent. It could increase the internal pressure of the PCR reagent and prevent the air gaps formation. This was because the high viscosity of the silicone oil would oppose the advancing movement of the silicone oil and the PCR reagent. At the same time, the gas bubbles generated at the back (by the electrolytic pump) would push the PCR reagent to move forward. As a result, the PCR reagent is compressed and the air gaps were eliminated.

4.2 Temperature Control

The relatively long equilibration time is due to the large thermal mass of the metal block. To reduce the duration for reaching the desired temperature, the size of the metal block should be reduced. By applying the same voltage, the duration for reaching the desired temperature would be reduced as the total thermal mass reduced. Besides, the applied voltage to the metal block could be increased. With the same thermal mass, the increase in the energy supply would decrease the duration for reaching the desired temperature.

In fact, for CFPCR, it is more crucial for the heater to maintain the desired constant temperature than to achieve a high temperature ramping rate. The temperature fluctuations of the three heaters were within 1 °C after reaching the desired temperatures. The small temperature fluctuations are due to the large thermal mass of the metal blocks. This is the reason of using metal blocks as heaters instead of using metal thin-films.

4.3 PCR Experiment

4.3.1 Effect of Silicone Oil

Nakayama' s group prevented bubbles generation in denaturation by introducing oil in front of PCR mixture. Using this method, the adsorption of the oil was observed in this study. Due to the hydrophobic property of PDMS, silicone oil adsorbed onto the inner surface of the CFPCR microchannel. During CFPCR, the amount of silicone oil in front of the PCR reagent decreased gradually and thus the opposing force to the PCR reagent would decrease. The flow rate of the PCR reagents increased. If all the silicone oil was adsorbed, the flow of the PCR reagents would be terminated. Therefore, sufficient amount of silicone oil was introduced to eliminate this effect. Besides, non-hydrophotic material could be used for the microchip. This can avoid the adsorption of the oil on the surface of the microchip. In addition, sensors could be added to monitor the flow rate of the reagents. The applied current could be varied to adjust the flow rate of the reagents.

4.3.2 Effect of Concentration of Taq DNA Polymerase

The results showed that the brightness of the PCR product bands was related to the concentration of the Taq DNA polymerase. The PCR product bands were brighter if the higher concentration of the Taq DNA Polymerase was used. Regarding to the Prakash's study, the contact angle of the PDMS decreased after incubation of Taq DNA polymerase. The reason was that Taq DNA polymerase was adsorbed onto the surface of the CFPCR microchannel due to the hydrophobic property of PDMS. This caused a decrease in free Taq DNA polymerase concentration and the amplification efficiency. With higher Taq DNA polymerase concentration (i.e., 2.5 units/20 μL), even though a significant portion could be adsorbed, free Taq DNA polymerase concentration is high enough to produce a bright PCR product band.

4.3.3 Effect of Surface Passivation

To compensate the adsorption of Taq DNA polymerase on the surface of CFPCR microchannel, the increase in concentration of Taq DNA polymerase was possible but it was expensive. Therefore, surface passivation, which was more cost effective, was performed in this study. When CFPCR was performed with dynamic passivation using BSA, the intensity of the PCR product band was much brighter than that without BSA. This suggested that dynamic passivation using BSA could reduce the adsorption of Taq DNA polymerase. Besides, the PCR product band intensity for 2 μg/μL BSA was similar to that for 0.5 μg/μL BSA. This indicated that dynamic passivation with 2 μg/μL BSA was optimal in this study. The amount of BSA was in excess if concentration of BSA was further increased.

Regarding to the static passivation, it should be noted that the intensity of the PCR product band for 5 μg/μL BSA was weaker than that for 2 μg/μL BSA. This can be explained by the fact that, at very high concentration of BSA static coating (i.e., 5 μg/μL), it is difficult to completely remove excess BSA from the entire CFPCR microchannel. The residue of the BSA would block the microchannel and the fluidic flow was unstable.

By considering the convenience of the passivation procedures, dynamic passivation is more suitable for practical application. This is because dynamic passivation only involves the addition of a PCR-friendly substance in the PCR reagent while static passivation involves the incubation and removal of the passivation agent which is time consuming. Besides, as discussed in the previous paragraph, incomplete removal of the passivation agent could result in unstable flow and hence lower the amplification efficiency.

4.3.4 Effect of CFPCR Duration

With CFPCR duration of 20 min, an observable PCR product band was obtained. This amplification time is much shorter than that of the conventional PCR thermal cycler. The results showed that the intensity of the PCR product band was brighter if the duration of CFPCR was longer. This also consists with Kopp's results. The fluorescence intensity increased if longer total cycling time was applied. This was because the longer duration allowed the sufficient time for the PCR, especially the extension process. Hence, this ensured the efficiency of the PCR.

4.3.5 Performance of Electrolytic Pump

CFPCR was performed successfully using the electrolytic pump. The PCR product band was obtained. To improve the brightness of the PCR product band, the concentration of the Taq DNA polymerase and the duration of CFPCR could be increased.

CHAPTER 5

CONCLUSIONS AND RECOMMENDATIONS

5.1 Conclusions

In this study, a CFPCR device with integrated on-chip electrolytic pump has been developed. It features simple microchip fabrication, small size, and short amplification time. A temperature control system was custom-built with metal heating blocks and feedback control, achieving accurate temperature control of ±1 °C. To optimize the DNA amplification efficiency of the CFPCR device, several parameters were studied including silicone oil plug in front of the PCR reagent, concentration of Taq DNA polymerase, as well as dynamic and static passivation with BSA. The presence of a silicone oil plug in front of the PCR reagent prevented evaporation and thus air gaps formation, which otherwise would seriously affect the fluid flow. The amplification efficiency of our CFPCR device was suppressed at Taq DNA polymerase concentrations of 1.5 units/20 μL and below due to non-specific adsorption onto the microchannel surface. Both dynamic and static passivation with BSA significantly reduced the adsorption, resulting in much higher amplification efficiency than without passivation. Successful amplification was achieved in about 20 min using electrolytic pump-driven CFPCR. In terms of fluid control, constant current produced more stable flow than constant voltage.

5.2 Recommendations for Future Work

First, the introduction of air into the reservoirs during the sealing process using polyimide film tape due to the elastic property of PDMS has to be addressed for widespread application. There are two possible solutions to this issue. One is to increase the hardness of PDMS by chemical modification. The simplest method is to increase the amount of curing agent during fabrication of PDMS. With less deformable PDMS, the air introduction during the sealing process will be alleviated. Another method is to replace PDMS with other hard materials such as poly(methylmethacrylate) (PMMA) and polycarbonate (PC). The main purpose of this study was to demonstrate the feasibility of using on-chip electrolytic pump for CFPCR. PDMS was chosen due to the ease of fabrication. The material can be replaced by other hard materials after this proof-of-concept demonstration.

Second, the adsorption of the silicone oil to the CFPCR microchannel surface is another issue worth further investigation. This could be addressed by modifying the surface of the microchannel to more hydrophilic. Another method is to replace the silicone oil to other viscous fluid which does not easily adsorbed onto the hydrophobic surface.

Third, the integration of this CFPCR device to other steps in DNA analysis has to be carried out. To date, only a few fully integrated DNA analysis systems with complete steps of sample preparation, amplification, and detection have been developed. Nevertheless, these systems are not very portable due to the bulky

supporting instrumentation for fluid handling and product detection (e.g., fluorescence measurement). Our CFPCR device with integrated on-chip electrolytic pump is conducive to a portable and fully integrated DNA analyzer. In terms of product detection, real-time electrochemical monitoring of the PCR amplicon generation can be easily achieved in CFPCR [34]. Efforts have to be made in isolating genomic DNA from raw sample on the same microchip platform.

REFERENCES

1. Urban, G.A., *BioMEMS*, 2006.
2. Mullis, K., Faloona, F., Scharf, S., Saiki, R., Horn, G., and Erlich, H., *Specific enzymatic amplification of DNA in vitro: The polymerase chain reaction.* Cold Spring Harbor Symposia on Quantitative Biology, 1986. **51**: p. 263–273.
3. Sun, Y. and Kwok, Y.C., *Polymeric microfluidic system for DNA analysis.* Analytica Chimica Acta, 2006. **556**(1): p. 80–96.
4. Zhang, C.S., Xu, J.L., Ma, W.L., and Zheng, W.L., *PCR microfluidic devices for DNA amplification.* Biotechnology Advances, 2006. **24**(3): p. 243–284.
5. Northrup, M.A., Gonzalez, C., Hadley, D., Hills, R.F., Landre, P., Lehew, S., Saw, R., Sninsky, J.J., and Watson, R., *A MEMS-based miniature DNA analysis system.* The 8th International Conference on Solid-state Sensors and Actuators, 1995. **1**: p. 764–767.
6. Poser, S., Schulz, T., Dillner, U., Baier, V., Köhler, J.M., Schimkat, D., Mayer, G., and Siebert, A., *Chip elements for fast thermocycling.* Sensors and Actuators A: Physical, 1997. **62**(1-3): p. 672–675.
7. Oda, R.P., Strausbauch, M.A., Huhmer, A.F.R., Borson, N., Jurrens, S.R., Craighead, J., Wettstein, P.J., Eckloff, B., Kline, B., and Landers, J.P.,

Infrared-mediated thermocycling for ultrafast polymerase chain reaction amplification of DNA. Analytical Chemistry, 1998. **70**(20): p. 4361–4368.

8. Roper, M.G., Easley, C.J., Legendre, L.A., Humphrey, J.A.C., and Landers, J.P., *Infrared temperature control system for a completely noncontact polymerase chain reaction in microfluidic chips.* Analytical Chemistry, 2007. **79**(4): p. 1294–1300.
9. El-Ali, J., Perch-Nielsen, I.R., Poulsen, C.R., Bang, D.D., Telleman, P., and Wolff, A., *Simulation and experimental validation of a SU-8 based PCR thermocycler chip with integrated heaters and temperature sensor.* Sensors and Actuators A: Physical, 2004. **110**(1-3): p. 3–10.
10. Mahjoob, S., Vafai, K., and Beer, N.R., *Rapid microfluidic thermal cycler for polymerase chain reaction nucleic acid amplification.* International Journal of Heat and Mass Transfer, 2008. **51**: p. 2109–2122.
11. Xiang, Q., Xu, B., Fu, R., and Li, D., *Real-time PCR on disposable PDMS chip with a miniaturized thermal cycler.* Biomedical Microdevices, 2005. **7**(4): p. 273–279.
12. Niu , Z.Q., Chen, W.Y., Shao, S.Y., Jia, X.Y., and Zhang, W.P., *DNA amplification on a PDMS–glass hybrid microchip.* Journal of Micromechanics and Microengineering, 2006. **16**(2): p. 425–433.
13. Kolari, K., Satokari, R., Kataja, K., Stenman, J., and Hokkanen, A., *Real-time analysis of PCR inhibition on microfluidic materials.* Sensors and Actuators B: Chemical, 2008. **128**(2): p. 442–449.

14. Cady, N.C., Stelick, S., Kunnavakkam, M.V., and Batt, C.A., *Real-time PCR detection of Listeria monocytogenes using an integrated microfluidics platform*. Sensors and Actuators B: Chemical, 2005. **107**(1): p. 332–341.

15. Zhang, C., Xing, D., and Li, Y., *Micropumps, microvalves, and micromixers within PCR microfluidic chips: Advances and trends*. Biotechnology Advances, 2007. **25**(5): p. 483–514.

16. Koh, C.G., Tan, W., Zhao, M.Q., Ricco, A.J., and Fan, Z.H., *Integrating polymerase chain reaction, valving, and electrophoresis in a plastic device for bacterial detection*. Analytical Chemistry, 2003. **75**(22): p. 6379–6379.

17. Ranjit , P.A., Adamia, S., Sieben, V., Pilarski, P., Pilarski, L.M., and Backhouse, C.J., *Small volume PCR in PDMS biochips with integrated fluid control and vapour barrier.* Sensors and Actuators B: Chemical, 2006. **113**(1): p. 398–409.

18. Cho, C.H., Cho, W., Ahn, Y., and Hwang, S.Y., *PDMS–glass serpentine microchannel chip for time domain PCR with bubble suppression in sample injection.* Journal of Micromechanics and Microengineering, 2007. **17**(9): p. 1810–1817.

19. Northrup, M.A., Benett, B., Hadley, D., Landre, P., Lehew, S., Richards, J., and Stratton, P., *A miniature analytical instrument for nucleic acids based on micromachined silicon reaction chambers.* Analytical Chemistry, 1998. **70**(5): p. 918–922.

20. Ibrahim, M.S., Lofts, R.S., Jahrling, P.B., Henchal, E.A., Weedn, V.W., Northrup, M.A., and Belgrader, P., *Real-time microchip PCR for detecting*

single-base differences in viral and human DNA. Analytical Chemistry, 1998. **70**(9): p. 2013–2017.

21. Christensen, T.B., Bang, D.D., and Wolff, A., *Multiplex polymerase chain reaction (PCR) on a SU-8 chip.* Microelectronic Engineering, 2008. **85**(5-6): p. 1278–1281.

22. Hagan, K.A., Reedy, C.R., Uchimoto, M.L., Basu, D., Engel, D.A., and Landers, J.P., *An integrated, valveless system for microfluidic purification and reverse transcription-PCR amplification of RNA for detection of infectious agents.* Lab on a Chip, 2011. **11**(5): p. 957–961.

23. Liu, R.H., Yang, J., Lenigk, R., Bonanno, J., and Grodzinski, P., Self-contained, fully integrated biochip for sample preparation, polymerase chain reaction amplification, and DNA microarray detection. Analytical Chemistry, 2004. 76(7): p. 1824–1831.

24. Kopp, M.U., de Mello, A.J., and Manz, A., *Chemical amplification: Continuous-flow PCR on a chip.* Science, 1998. **280**(5366): p. 1046–1048.

25. Li, Y.Y., Zhang, C.S., and Xing, D., *Integrated microfluidic reverse transcription-polymerase chain reaction for rapid detection of food- or waterborne pathogenic rotavirus.* Analytical Biochemistry, 2011. **415**(2): p. 87–96.

26. Zhang, C.S., and Xing, D., *Parallel DNA amplification by convective polymerase chain reaction with various annealing temperatures on a thermal gradient device*. Analytical Biochemistry, 2009. **387**(1): p. 102–112.

27. Chen, P.C., Fan, W., Hoo, T.K., Chan, C.Z., and Wang, Z., *Simulation guided-design of a microfluidic thermal reactor for polymerase chain reaction*. Chemical Engineering Research and Design, 2012. **90**(5): p. 591–599.

28. Tsai, N.C., and Sue, C.Y., 5. *SU-8 based continuous-flow RT-PCR bio-chips under high precision temperature control*. Biosensors and Bioelectronics, 2006. **22**: p. 313–317.

29. Felbel, J., Reichert, A., Kielpinski, M., Urban, M., Henkel, T., Hafner, N., Durst, M., and Weber, J., *Reverse transcription-polymerase chain reaction (RT-PCR) in flow through micro reactors Thermal and fluidic concepts*. Chemical Engineering Journal, 2008. **135**: p. 298–302.

30. Felbel, J., Reichert, A., Kielpinski, M., Urban, M., Hafner, N., Durst, M., Kohler, J.M., Weber, J., and Henkel, T., *Technical concept of a flow-through microreactor for in-situ RT-PCR*. Engineering in Life Sciences, 2008. **8**(1): p. 68–72.

31. Hartung, R., Brosing, A., Sczcepankiewicz, G., Liebert, U., Hafner, N., Durst, M., Felbel, J., Lassner, D., Kohler, J.M., *Application of an asymmetric helical tube reactor for fast identification of gene transcripts of pathogenic viruses by micro flow-through PCR*. Biomed Microdevices, 2009. **11**(3): p. 685–692.

32. Park, N., Kim, S., and Hahn, J.H., *Cylindrical compact thermal-cycling device for continuous-flow polymerase chain reaction*. Analytical Chemistry, 2003. **75**(21): p. 6029–6033.

33. Li, Y., Xing, D., and Zhang, C.S., *Rapid detection of genetically modified organisms on a continuous flow polymerase chain reaction microfluidics*. Analytical Biochemistry, 2009. **385**(1): p. 42–49.

34. Curcio, M., and Roeraade, J., *Continuous segmented-flow polymerase chain reaction for high throughput miniaturized dna amplification*. Analytical Chemistry, 2003. **75**(1): p. 1–7.

35. Peham, R., Grienauer, W., Steiner, H., Heer, R., Vellekoop, J., and Nohammer, C., *Long target droplet polymerase chain reaction with a microfluidic device for high throughput detection of pathogenic bacteria at clinical sensitivity*. Biomed Microdevices, 2011. **13**(3): p. 463–473.

36. Gonzalez, A., Ciobanu, D., Sayers, M., Sirr, N., Dalton, T., and Davies, M., *Gene transcript amplification from cell lysates in continuous-flow microfluidic devices*. Biomed Microdevices, 2007. **9**(5): p. 729–736.

37. Dorfman, K.D., Chabert, M., Codarbox, J.H., Rousseau, G., Cremoux, P.D., and Viovy, J.L., *Contamination-free continuous flow microfluidic polymerase chain reaction for quantitative and clinical applications*. Analytical Chemistry, 2005. **77**(11): p. 3700–3704.

38. Chabert, M., Dorfman, K.D., Cremoux, P.D., Roeraade, J., and Viovy, J.L., *Automated microdroplet platform for sample manipulation and polymerase chain reaction*. Analytical Chemistry, 2006. **78**(22): p. 7722–7728.

39. Zhang, C.S., Xu, J.L., Wang, J.Q., and Wang, H.Y., *Continuous-flow polymerase chain reaction microfluidics based on polytetrafluoethylene capillary*. Chinese Journal of Analytical Chemistry, 2006. **34**(8): p. 1197–1202.

40. Zhang, C.S., Xu, J.L., Wang, J.Q., and Wang, H.Y., *Rapid amplification and detection of foodborne pathogenic rotavirus by continuous-flow reverse transcription-polymerase chain reaction integrated with online fluorescence analysis*. Chinese Journal of Analytical Chemistry, 2011. **39**(5): p. 645–651.

41. Sun, Y., Satyanarayan, M.V.D., Nauyen, N.T., and Kwok, Y.C., *Continuous flow polymerase chain reaction using a hybrid PMMA-PC microchip with improved heat tolerance*. Sensors and Actuators B, 2008. **130**(2): p. 836–841.

42. Kim, J.A., Lee, J.Y., Seong, S., Cha, S.H., Lee, S.H., Kim, J.J., and Park, T.H., *Fabrication and characterization of a PDMS–glass hybrid continuous-flow PCR chip*. 2006. **29**(1–2): p. 91–97.

43. Wang, J.H., Chien, L.J., Hsieh, T.M., Luo, C.H., Chou, W.P., Chen, P.H., Chen, P.J., Lee, D.S., and Lee, G.B., *A miniaturized quantitative polymerase chain reaction system for DNA amplification and detection*. Sensors and Actuators B, 2009. **141**(1): p. 329–337.

44. Sun, K., Yamaguchi, A., Ishida, Y., Matsuo, S., and Misawa, H., *A heater-integrated transparent microchannel chip for continuous-flow PCR*. Sensors and Actuators B, 2001. 84(2–3): p. 283–289.

45. Obeid, P.J., and Christopoulos, T.K., *Continuous-flow DNA and RNA amplification chip combined with laser-induced fluorescence detection*. Analytica Chimica Acta, 2003. **494**(1–2): p. 1–9.

46. Reichert, A., Felbel, J., Kelpinski, M., Urban, M., Steinbrecht, B., and Henkel, T., *Micro flow-through thermocycler with simple meandering channel with symmetric temperature zones for disposable PCR-devices in microscope slide format*. Journal of Bionic Engineering, 2008. **5**(4): p. 291–298.

47. Mavraki, E., Moschou, D., Kokkoris, G., Vourdas, N., Chatzandroulis, S., and Tserepi, A., *A continuous flow μPCR device with integrated microheaters on a flexible polyimide substrate*. Procedia Engineering, 2011. **25**: p. 1245–1248.

48. Chen, P.C., Park, D.S., You, B.H., Kim, N., Park, T., Soper, S.A., Nikitopoulos, D.E., and Murphy, M.C., *Titer-plate formatted continuous flow thermal reactors Design and performance of a nanoliter reactor*. Sensors and Actuators B, 2010. **149**(1): p. 291–300.

49. Yu, C.Y., Liang, W.S., Kuan, I, Wei, C.H., and Gu, W.G., *Fabrication and characterization of a flow-through PCR device with integrated chromium*

resistive heaters. Journal of the Chinese Institute of Chemical Engineers, 2007. **38**(3–4): p. 333–339.

50. Kuan, I., Gu, W.G., Wu, J.C., Wei, C.H., Chen, K.S., and Yu, C.Y., *Effects of grafting poly(ethylene oxide) on the amplification efficiency of a poly(dimethylsiloxane)-based flow-through PCR device*. Chemical Engineering Journal, 2008. **143**(1–3): p. 326–330.

51. Hashimoto, M., Barany, F., and Soper, S.A., *Polymerase chain reaction ligase detection reaction hybridization assays using flow through microfluidic devices for the detection of low abundant DNA point mutations*. Biosensors and Bioelectronics, 2006. **21**(10): p. 1915–1923.

52. Tan, H.H., Trinh, K.T.L., and Lee, N.Y., *Pressure-driven one-step solid phase-based on-chip sample preparation on a microfabricated plastic device and integration with flow-through polymerase chain reaction (PCR).* Journal of Chromatography B, 2013.

53. Liu, D.Y., Liang, G.T., Lei, X.X., Chen, B., Wang, W., and Zhou, X.M., *Highly efficient capillary polymerase chain reaction using an oscillation droplet microreactor*. Analytica Chimica Acta, 2012. **718**: p. 58–63.

54. West, J., Karamata, B., Lilis, B., Gleeson, J.P., Alderman, J., Collins, J.K., Lane, W., Mathewson, A., and Berney, H., *Application of magnetohydrodynamic actuation to continuous flow chemistry*. Lab on a Chip, 2002. **2**: p. 224–230.

55. Chiou, J., Matsudaira, P., Sonin, A., and Ehrlich, D., *A Closed-Cycle Capillary Polymerase Chain Reaction Machine. Analytical Chemistry*, 2001. **73**(9): p. 2018–2021.

56. Nakano, H., Matsuda, K., Yohda, M., Nagamune, T., Endo, I., and Yamane, T., *High Speed Polymerase Chain Reaction in Constant Flow*. Bioscience, Biotechnology, and Biochemistry, 1994. **58**(2): p 349–352.

57. Bu, M., Melvin, T., Ensell, G., Wilkinson, J.S., and Evans, A.G.R., *Design and theoretical evaluation of a novel microfluidic device to be used for PCR*. Journal of Micromechanics and Microengineering, 2003. **13**(4): p. 125–130.

58. Fukuba, T., Yamamoto, T., Naganuma, T., and Fujii, T., 35. *Microfabricated flow-through device for DNA amplification-towards in situ gene analysis*. Chemical Engineering Journal, 2004. **101**: p 151–156.

59. Wang, W. Li, Z.X., Yang, Y.J., and Guo, Z.Y., *Droplet based micro oscillating flow-through PCR chip*. Micro Electro Mechanical Systems, 2004. p.280–283.

60. Chen, Z.Y., Qian, S.Z., Abrams, W.R., Malamud, D., and Bau, H.H., *Thermosiphon-Based PCR Reactor Experiment and Modeling*. Analytical Chemistry, 2004. **76**(13): p.3707–3715.

61. Krishnam, M., Ugaz, V.M., Burns, M.A., *PCR in a Rayleigh-Bénard convection cell*. Science, 2002. **298**: p.793.

62. Liu, J., Enzelerger, M., and Quake, S., *A nanoliter rotary device for polymerase chain reaction*. Electrophoresis, 2002. **23**(10): p. 1531–1536.

63. Jia, X.Y., Niu, Z.Q., and Chen, W.Y., A Rotary Polydimethylsiloxane-Based Device for Polymerase Chain Reaction. Analytical Letters, 2005. **38**(13): p. 2143–2149.

64. Li, S.F., Fozdar, Y., Ali, M.F., Li, H., Shao, D.B., Vykoukal, D.M., Vykoukal, J., Floriano, P.N., Olsen, M., McDvitt, J.T., Gascoyne, R.C., and Chen, S.C., 41. *A continuous-flow polymerase chain reaction microchip with regional velocity control*. Journal of Microelectromechanical Systems, 2006. **15**(1): p. 223–236.

65. Schaerli, Y., Wootton, R.C., Robinson, T., Stein, V., Dunsby, C., Neil, A.A., French, M.W., deMello, A.J., Abell, C., and Hollfelder, F., *Continuous-flow polymerase chain reaction of single copy dna in microfluidic microdroplets*. Analytical Chemistry, 2009. **81**(1): p. 302–306.

66. Crews, N., Wittwer, C., and Gale, B., *Continuous-flow thermal gradient PCR. Biomed Microdevices*, 2008. 10(2): p. 187–195.

67. Gartner, C., Klemm, R., and Becker, H., *Methods and instruments for continuous-flow PCR on a chip*. Microfluidics, BioMEMS, and Medical Microsystems V, 2007. **6465**.

68. Hashimoto, M., Chen, P.C., Mitchell, M.W., Nikitopoulos, D.E., Soper, S.A., and Murphy, M.C., *Rapid pcr in a continuous flow device*. Lap on a Chip, 2004. **4**(6): p 638–45.

69. The, H.F., Naveen, R., Dong, X.D., Tan, S.N., Zeng, X.T., Tan, L.K., Yap, P.H., and Gong, H.Q., *Real-time PCR microfluidic devices with concurrent electrochemical detection*. Biosensors and Bioelectronics, 2009. **24**(7): p. 2131–2136.

70. Fuchiwaki, Y., Nagai, H, Saito, M., and Tamiya, E, *Ultra-rapid flow-through polymerase chain reaction microfluidics using vapor pressure*. Biosensors and Bioelectronics, 2011. **27**(1): p. 88–94.

71. Nakano, K., Hino, A., Yamamura, S., Takamura, Y., and Tamiya, E., *Circumventing air bubbles in microfluidic systems and quantitative continuous-flow PCR applications.* Analytical and Bioanalytical Chemistry, 2006. **386**(5): p. 1327–1333.

72. Wang, H., Chen, J., Zhu, L., Shadpour, H., Hupert, M.L., and Soper, S.A., C*ontinuous flow thermal cycler microchip for DNA cycle sequencing.* Analytical Chemistry, 2006. **78**(17): p. 6223–6231.

73. Chen, J., Wabuyele, M., Chen, H., Patterson, D., Hupert, M., Shadpour, H., Nikitopoulos, D., and Soper, S.A., *Electrokinetically synchronized polymerase chain reaction microchip fabricated in polycarbonate*. Analytical Chemistry, 2005. **77**(2): p. 658–666.

74. Joung, S.R., Kim, J., Choi, Y.J., Kang, C.J., and Kim, Y.S., *ITO-coated glass polydimethylsiloxane continuous-flow PCR chip*. Proceddings of the 2nd IEEE International Conference on Nano/Micro Engineered and Molecular Systems, 2007.

75. Yao, L.Y., Liu, B., Chen, T., Liu, S.B., and Zuo, T.C., *Micro flow-through PCR in a PMMA chip fabricated by KrF excimer lase*. Biomedical Microdevices, 2005. **7**(3): p. 253–257.

76. Lok, K.S., Lee, P.F., Kwok, Y.C., and Nguyen, N.T., *Nested PCR in magnetically actuated circular closed-loop PCR microchip system.* Microchimica Acta, 2012. **177**(1–2): p. 111–117.

77. Cheng, J.Y., Hsieh, C.J., Chuang, Y.C., and Hsieh, J.R., *Performing microchannel temperature cycling reactions using reciprocating reagent shuttling along a radial temperature gradient.* The Analyst, 2005. **130**(6): p. 931–940.

78. Jia, X.Y., Niu, Z.Q., Chen, W.Y., and Zhang, W.P., 56. *Polydimethylsiloxane (PDMS)-based spiral channel PCR chip.* Electronics Letters, 2005. **41**(16): p. 890–891.

79. Crews, N., Wittwer, C., Palais, R., and Gale, B., *Product differentiation during continuous-flow thermal gradient PCR.* Lab on a Chip, 2008. **8**(6): p. 919–924.

80. Polini, A., Mele, E., Sciancalepore, A.G., Girardo, S., Biasco, A., Camposeo, A., Cingolani, R., Weitz, D.A., and Pisignano, D., *Reduction of water evaporation in polymerase chain reaction microfluidic devices based on oscillating-flow.* Biomicrofluidics, 2010. **4**(3): p. 1–10.

81. Wang, H.Y., Zhang, C.S., and Xing, D., *Simultaneous detection of Salmonella enterica, Escherichia coli O157 H7, and Listeria monocytogenes using oscillatory-flow multiplex PCR. Microchimica Acta*, 2011. **173**(3–4): p. 503–512.

82. Zhang, C.S. and Xing, D., *Miniaturized PCR chips for nucleic acid amplification and analysis: Latest advances and future trends.* Nucleic Acids Research, 2007. **35**(13): p. 4223–4237.

83. Chien, C.H. and Yu, H.M., *The design and fabrication of polymerase chain reaction platform.* Microsystem Technologies, 2007. **13**(11): p. 1523–1527.

84. Chen, P.C., Nikitopoulos, D., Soper, S., and Murphy, M., *Temperature distribution effects on micro-CFPCR performance.* Biomedical Microdevices, 2008. **10**(2): p. 141–152.

85. Moeller, K., Besecker, J., Hampikian, G., Moll, A., Plumlee, D., Youngsman, J., and Hampikian, J.M. *A prototype continuous flow polymerase chain reaction LTCC device*. 5th International Conference on Processing and Manufacturing of Advanced Materials, 2006.

86. Kong, D., Kang, T., Seo, C., Cho, C., and Lee, J., *Fabrications of a continuous-flow DNA amplifier using dry film resist.* BioChip Journal, 2010. **4**(3): p. 179–183.

87. Pješčić, I., Tranter, C., Hindmarsh, P., and Crews, N., *Glass-composite prototyping for flow PCR with in situ DNA analysis.* Biomedical Microdevices, 2010. **12**(2): p. 333–343.

88. Schneega, I., Brautigam, R., and Kohler, J.M., *Miniaturized flow-through PCR with different template types in a silicon chip thermocycler.* Lab on a Chip, 2001. **1**(1): p. 42–49.

89. Obeid, P.J., Christopoulos, T.K., Crabtree, H.J., and Backhouse, C.J., *Microfabricated device for DNA and RNA amplification by continuous-flow polymerase chain reaction and reverse transcription-polymerase chain reaction with cycle number selection.* Analytical Chemistry, 2003. **75**(2): p. 288–295.

90. Schaerli, Y., Wootton, R.C., Robinson, T., Stein, V., Dunsby, C., Neil, A.A., French, M.W., deMello, J., Abell, C., and Hollfelder, F., *Continuous-flow polymerase chain reaction of single-copy DNA in microfluidic microdroplets.* Analytical Chemistry, 2008. **81**(1): p. 302–306.

91. Sun, Y., Kwok, Y.C., and Nguyen, N.T., *A circular ferrofluid driven microchip for rapid polymerase chain reaction.* Lab on a Chip, 2007. **7**(8): p. 1012–1017.

92. Wang, C.H., Chen, Y.Y., Liao, C.S., Hsieh, T.M., Luo, C.H., J., W.J., Lee, H.H., and Lee, G.B., *Circulating polymerase chain reaction chips utilizing*

multiple-membrane activation. Journal of Micromechanics and Microengineering, 2007. **17**(2): p. 367–375.

93. Chung, K.H., Park, S.H., and Choi, Y.H., *A palmtop PCR system with a disposable polymer chip operated by the thermosiphon effect.* Lab on a Chip, 2010. **10**(2): p. 202–210.

94. Li, Y.Y., Zhang, C.S., and Xing, D., *Fast identification of foodborne pathogenic viruses using continuous-flow reverse transcription-PCR with fluorescence detection.* Microfluidics and Nanofluidics, 2011. **10**(2): p. 367–380.

95. Park, S.W., *Titer plate formatted continuous flow thermal reactors for high throughput applications: Fabrication and testing.* Journal of Micromechanics and Microengineering, 2010. **20**(5): p. 1–11.

96. Wilding, P., Shoffner, M.A., and Kricka, L.J., *PCR in a silicon microstructure.* Clinical Chemistry, 1994. **40**(9): p. 1815–1818.

97. Erill, I., Campoy, S., Erill, N., Barbé, J., and Aguiló, J., *Biochemical analysis and optimization of inhibition and adsorption phenomena in glass–silicon PCR-chips.* Sensors and Actuators B: Chemical, 2003. **96**(3): p. 685–692.

98. Prakash, A., Amrein, M., and Kaler, K., *Characteristics and impact of Taq enzyme adsorption on surfaces in microfluidic devices.* Microfluidics and Nanofluidics, 2008. **4**(4): p. 295–305.

99. Rodriguez, I., Lesaicherre, M., Tie, Y., Zou, Q., Yu, C., Singh, J., Meng, L.T., Uppili, S., Li, S.F.Y., Gopalakrishnakone, P., and Selvanayagam, Z.E.,

Practical integration of polymerase chain reaction amplification and electrophoretic analysis in microfluidic devices for genetic analysis. Electrophoresis, 2003. **24**(1–2): p. 172–178.

100. Shoffner, M.A., Cheng, J., Hvichia, G.E., Kricka, L.J., and Wilding, P., *Chip PCR. I. Surface passivation of microfabricated silicon–glass chips for PCR.* Nucleic Acids Research, 1996. **24**(2): p. 375–379.

101. Friedman, N.A. and Meldrum, D.R., *Capillary tube resistive thermal cycling.* Analytical Chemistry, 1998. **70**(14): p. 2997–3002.

102. Xia, Y.M., Hua, Z.S., Srivannavit, O., Ozel, A.B., and Gulari, E., *Minimizing the surface effect of PDMS–glass microchip on polymerase chain reaction by dynamic polymer passivation.* Journal of Chemical Technology & Biotechnology, 2007. **82**(1): p. 33–38.

103. Nisar, A., AftuIpurkar, N., Mahaisavariya, B., and Tuantranont, A., *MEMS-based micropumps in drug delivery and biomedical applications.* Sensors and Actuators B: Chemical, 2008. **130**(2): p. 917–942.

104. Huang, F.C., Liao, C.S., and Lee, G.B., *An integrated microfluidic chip for DNA/RNA amplification, electrophoresis separation and on-line optical detection.* Electrophoresis, 2006. **27**(16): p. 3297–3305.

105. Easley, C.J., Karlinsey, J.M., and Landers, J.P., *On-chip pressure injection for integration of infrared-mediated DNA amplification with electrophoretic separation.* Lab on a Chip, 2006. **6**(5): p. 601–610.

106. Cameron, C.G. and Freund, M.S., *Electrolytic actuators: Alternative, high-performance, material-based devices.* Proceedings of the National Academy of Sciences of the United States of America, 2002. **99**(12): p. 7827–7831.

107. Suzuki, H. and Yoneyama, R., *A reversible electrochemical nanosyringe pump and some considerations to realize low-power consumption.* Sensors and Actuators B: Chemical, 2002. **86**(2-3): p. 242–250.

108. Chiu, S.H. and Liu, C.H., *An air-bubble-actuated micropump for on-chip blood transportation.* Lab on a Chip, 2009. **9**(11): p. 1524–1533.

109. Munyan, J.W., Fuentes, H.V., Draper, M., Kelly, R.T., and Woolley, A.T., *Electrically actuated, pressure-driven microfluidic pumps.* Lab on a Chip, 2003. **3**(4): p. 217–220.

110. Blanco-Gomez, G., Glidle, A., Flendrig, L.M., and Cooper, J.M., *Integration of low-power microfluidic pumps with biosensors within a laboratory-on-a-chip device.* Analytical Chemistry, 2009. **81**(4): p. 1365–1370.

111. Furdui, V.I., Kariuki, J.K., and Harrison, D.J., *Microfabricated electrolysis pump system for isolating rare cells in blood.* Journal of Micromechanics and Microengineering, 2003. **13**(4): p. S164 –S170.

112. Saati, S., Lo, R., Li, P.Y., Meng, E., Varma, R., and Humayun, M.S., *Mini drug pump for ophthalmic use.* Current Eye Research, 2010. **35**(3): p. 192–201.

113. Kabata, A., Okamura, K., Suzuki, H., Kishigami, Y., Kikuchi, M., and Haga, M., *Prototype micropump for insulin administration based on*

electrochemical bubble formation. Journal of Pharmaceutical Sciences, 2008. **97**(11): p. 5037–5045.

114. Xie, J., Miao, Y., Shih, J., He, Q., Liu, J., Tai, Y.C., and Lee, T.D., *An electrochemical pumping system for on-chip gradient generation.* Analytical Chemistry, 2004. **76**(13): p. 3756–3763.

115. Böhm, S., hm, S., Olthuis, W., and Bergveld, P., *An integrated micromachined electrochemical pump and dosing system.* Biomedical Microdevices, 1998. **1**: p. 121–130.

116. Böhm, S., Timmer, B., Olthuis, W., and Bergveld, P., *A closed-loop controlled electrochemically actuated micro-dosing system.* Journal of Micromechanics and Microengineering, 2000. **10**(4): p. 498–504.

117. Li, P.Y., Shih, J., Lo, R., Adams, B., Agrawal, R., Saati, S., Humayun, M.S., Tai, Y.C., and Meng, E., *An electrochemical intraocular drug delivery device.* Sensors and Actuators A: Physical, 2007. **143**: p. 206–209.

118. Nakayama, T., Hiep, H., Furui, S., Yonezawa, Y., Saito, M., Takamura, Y., and Tamiya, E., *An optimal design method for preventing air bubbles in high-temperature microfluidic devices.* Analytical and Bioanalytical Chemistry, 2010. **396**(1): p. 457–464.

119. Wu, W., Kang, K.T., and Lee, N.Y., *Bubble-free on-chip continuous-flow polymerase chain reaction: Concept and application.* Analyst, 2011. **136**(11): p. 2287–2293.

120. Green, J.V., Kniazeva, T., Abedi, M., Sokhey, D.S., Taslim, M.E., and Murthy, S.K., *Effect of channel geometry on cell adhesion in microfluidic devices.* Lab on a Chip, 2009. **9**(5): p. 677–685.